Population genomics of bank vole populations reveals associations between immune related genes and the epidemiology of Puumala hantavirus in Sweden

Audrey Rohfritsch[1]#, Maxime Galan[1]#, Mathieu Gautier[1], Karim Gharbi[2], Gert Olsson[3], Bernhard Gschloessl[1], Caroline Zeimes[4], Sophie VanWambeke[4], Renaud Vitalis[1], Nathalie Charbonnel[1*]

[1] CBGP, INRA, CIRAD, IRD, Montpellier SupAgro, Univ. Montpellier, Montpellier, France. E-mail: nathalie.charbonnel@inra.fr

[2] Genome Science, Edinburgh Genomics, Ashworth Laboratories, The University of Edinburgh, Edinburgh, EH9 3FL, UK

[3] Department of Wildlife, Fish, and Environmental Studies, SLU, SE- 901 83 Umeå, Sweden

[4] Georges Lemaître Centre for Earth and Climate Research, Earth and Life Institute, Université Catholique de Louvain (UCL), Louvain-la-Neuve, Belgium

#These authors contributed equally to this work.

Keywords: RAD-sequencing, adaptation, hantavirus, voles, molecular epidemiology, selection

*Corresponding author: Charbonnel Nathalie, 750 avenue du campus Agropolis, *CS 30016, F-34988 Montferrier-sur-Lez, France. Fax : +0033 (0)4 99 62 33 45.* E-mail: nathalie.charbonnel@inra.fr

Running title: Bank vole population genomics and hantavirus

Abstract

Infectious pathogens are major selective forces acting on individuals. The recent advent of high-throughput sequencing technologies now enables to investigate the genetic bases of resistance/susceptibility to infections in non-model organisms. From an evolutionary perspective, the analysis of the genetic diversity observed at these genes in natural populations provides insight into the mechanisms maintaining polymorphism and their epidemiological consequences. We explored these questions in the context of the interactions between Puumala hantavirus (PUUV) and its reservoir host, the bank vole *Myodes glareolus*. Despite the continuous spatial distribution of *M. glareolus* in Europe, PUUV distribution is strongly heterogeneous. Different defence strategies might have evolved in bank voles as a result of co-adaptation with PUUV, which may in turn reinforce spatial heterogeneity in PUUV distribution. We performed a genome scan study of six bank vole populations sampled along a North/South transect in Sweden, including PUUV endemic and non-endemic areas. We combined candidate gene analyses (*Tlr4*, *Tlr7*, *Mx2* genes) and high throughput sequencing of RAD (Restriction-site Associated DNA) markers. We found evidence for outlier loci showing high levels of genetic differentiation. Ten outliers among the 52 that matched to mouse protein-coding genes corresponded to immune related genes and were detected using ecological associations with variations in PUUV prevalence. One third of the enriched pathways concerned immune processes, including platelet activation and TLR pathway. In the future, functional experimentations should enable to confirm the role of these these immune related genes with regard to the interactions between *M. glareolus* and PUUV.

Introduction

Infections are among the strongest selective forces acting in natural populations (Fumagalli et al., 2011; Karlsson, Kwiatkowski, & Sabeti, 2014). As a consequence, hosts have evolved a wide range of defence mechanisms against their pathogens. Understanding variation in host defence mechanisms has been at the core of eco-immunology in the last two decades (Sheldon & Verhulst, 1996). This immuno-heterogeneity seems to be strongly driven by non-heritable influences (e.g., age, physiological status, resource availability, microbial exposure, history of infections during lifetime, Schmid-Hempel, 2003; Schulenburg, Kurtz, Moret, & Siva-Jothy, 2009). It also has a genetic basis that is highly correlated to immune-related genes (Barreiro & Quintana-Murci, 2010; Hill et al., 1994). In this context, population genetics approaches may help deciphering the relative influence of different evolutionary processes (including migration, drift, and selection) in shaping the variation of immune-related genes in space and time (Charbonnel & Cosson, 2011; Quintana-Murci & Clark, 2013). In turn, the analysis of the genetic diversity observed at immune-related genes in natural populations enables to elucidate some geographical patterns of pathogen distribution. Still, only few studies address the question of how pathogen-mediated selective processes in the hosts may shape the spatial distribution of pathogens but see (Guivier, Galan, Henttonen, Cosson, & Charbonnel, 2014; Guivier et al., 2010; Wenzel, Douglas, James, Redpath, & Piertney, 2016).

A particularly relevant study system to tackle these questions consists of the interaction between the hantavirus Puumala (PUUV), the causative agent of nephropathia epidemica in humans (Brummer-Korvenkotio, Henttonen, & Vaheri, 1982), and its reservoir host, the bank vole *Myodes glareolus*. Despite the continuous

spatial distribution of *M. glareolus* in Europe (Stenseth, 1985), PUUV distribution is strongly heterogeneous (Olsson, Leirs, & Henttonen, 2010). Different hypotheses have been sought to explain this discrepancy. First, environmental variables that affect bank vole population size, e.g. landscape fragmentation or low snow cover, are likely to affect PUUV epidemiology and prevent PUUV persistence within reservoir host populations. They may at least partly explain the absence of PUUV in particular geographic areas. Second, environmental factors may also affect the possibility for PUUV to survive outside its reservoir host (e.g. low soil humidity or high temperatures, Sauvage, Langlais, Yoccoz, & Pontier, 2003). However, ecological niche modelling based on these environmental variables failed to explain accurately the distribution of PUUV in Europe (Zeimes, Olsson, Ahlm, & Vanwambeke, 2012; Zeimes et al., 2015). An alternative hypothesis states that spatial variation in the outcomes of *M. glareolus* / PUUV interactions may affect PUUV replication and excretion in the environment, which could ultimately shape PUUV distribution and nephropathia epidemica incidence in Europe (Guivier et al., 2014; Rohfritsch, Guivier, Galan, Chaval, & Charbonnel, 2013). Indeed, voles differ in their probability of being infected by PUUV (Kallio et al., 2006) and experimental infections have confirmed that the outcome of PUUV infection could vary between individuals (Dubois, Castel, et al., 2017; Hardestam et al., 2008). Furthermore, the genetic background of bank voles contributes to the variation in the response to infection (Charbonnel et al., 2014). In particular, differences in SNP allele frequencies within the tumor necrosis factor (*Tnf*) promoter and the *Mx2* gene are likely to influence PUUV distribution and epidemiology (Guivier et al., 2014; Guivier et al., 2010).

So far, the role of immune-related genes on bank vole response to PUUV infection has only been investigated for a handful of candidate genes (Charbonnel et al., 2014). The

recent advent of high-throughput sequencing technologies now offers the opportunity to test for associations between genetic polymorphisms and susceptibility to infections in natural populations, at a genome-wide scale. Here, we focus on bank vole populations from Sweden, a relevant geographic area for the purpose of this study since the distribution of PUUV is highly heterogeneous throughout the country. Nephropathia epidemica is endemic in the central and northern parts of the country (Niklasson & LeDuc, 1987), with about 90% of all human cases in Sweden being found in the four northernmost counties. In particular, Västerbotten county exhibits the highest nephropathia epidemica incidence in Sweden, and probably even worldwide (Petterson, Boman, Juto, Evander, & Ahlm, 2008). This geographic pattern is not explained by the reservoir distribution because the bank vole is also common in the South of Sweden (Hörling et al., 1996). Furthermore, Sweden is characterized by a wide range of climatic and ecological conditions, which influence the spatial vegetation pattern. In particular, the landscape forest is divided in several vegetation zones, from the nemoral zone in the south where broad-leved deciduous forests dominate, the hemiboreal transition with mixed deciduous and coniferous forests to the northern wide belt of boreal forests, and up to the arctic tundra in the north. Finally, there is a contact zone at around 63° N in Sweden where two subpopulations of *M. glareolus* characterized by differentiated mitochondrial lineages meet (Nemirov, Leirs, Lundkvist, & Olsson, 2010). It is assumed that this contact zone was established during the Late Weichselian deglaciation, when bank voles re-colonized the Scandinavian Peninsula through a first, South-Scandinavian, migration stream across a pre-historic land bridge from present Denmark, and a second migration stream from the North-East (Tegelstrom, 1987). It has been shown that the PUUV strains present in the northern bank vole population are differentiated from those

161 circulating in the southern bank vole populations (Hörling et al., 1996; Johansson et al.,
162 2008).

163 The main objective of the present study was to characterize genome-wide patterns of
164 bank vole population differentiation along a North/South transect in Sweden, and to
165 identify specific genomic regions showing footprints of divergent selection between
166 PUUV endemic areas in the North and non-endemic areas in the South. To that end, we
167 used a population genomics approach relying on the sequencing of restriction-site-
168 associated DNA (RAD-seq, see Baird et al., 2008) of pools of DNA from individuals
169 sampled in six different localities and that have previously been characterized for a set
170 of candidate genes (Dubois, Galan, et al., 2017). We combined different model-based
171 methods of genome-scan, that allowed us to consider several underlying demographic
172 scenarios, as well as putative associations with environmental variables. Last, we
173 specifically asked whether immune-related genes were overrepresented among the
174 genomic regions identified as presumably targeted by selection, as expected under the
175 hypothesis that bank vole defence strategies against PUUV may have evolved differently
176 in PUUV endemic and non-endemic areas. Overall, our study provides new insights into
177 the selective processes that are likely to be involved in *M. glareolus* / PUUV interactions,
178 and the mechanisms underlying the defence strategies of *M. glareolus* against PUUV
179 infections. As such, it contributes to a better understanding of the factors driving PUUV
180 distribution in reservoir populations, which is an important pre-requisite to apprehend
181 the risk of nephropathia epidemica in Sweden.

182

183 **Materials and methods**

184 *Sampling*

Sampling was performed in April and October 2012. Using snap trapping, a total of 257 bank voles were caught in six localities distributed along a transect running from the North of Sweden, which is known to be highly endemic for PUUV, to the South of Sweden, where PUUV is absent in both bank voles and humans (Fig. 1, Table 1). Collected voles were kept on ice and transferred to -20°C freezers, before being processed in the laboratory. A piece of hind foot was placed in 95 % ethanol for further analyses. Permission to trap voles was obtained from the Swedish Environmental Protection Agency (SEPA; latest permission: Dnr 412-4009-10) and from the Animal Ethics Committee in Umeå (latest permission: Dnr A-61-11).

Molecular markers

Genomic DNA was extracted using the EZ-10 96-well plate genomic DNA isolation Kit for animal samples (Bio Basic Inc.) following the manufacturer recommendations.

Immune-related candidate genes: we studied the polymorphism of immune-related genes that have previously been shown to be associated with PUUV infections (Tnf promoter, Mx2, Tlr4 and Tlr7 genes, see for a review Charbonnel et al., 2014). The detection of polymorphisms in *Tnf* promoter was assessed using primers and PCR conditions derived from Guivier et al. (2010). For all other candidate genes, sequences of rat and mouse (*Mx2* exons 13 and 14 cDNA, *Tlr4* cDNA, and *Tlr7* cDNA) were retrieved from the Ensembl website (see Suppl. Mat. Table S1 for accession numbers). Specific primers were developed for all immune genes in Primer Designer - version 2.0 (Scientific and educational Software Program 1991). Because the exon 3 of *Tlr*s could not be sequenced at once (2251bp for *Tlr4*, 3149bp for *Tlr7*), we designed two primer sets to sequence two fragments of about 1000 bp for each *Tlr* (see Suppl. Mat. Table S2

209 for primer sequences). We first assessed polymorphism based on 12 bank voles. PCRs
210 were performed on an Eppendorf Mastercycler EPgradient S (Hamburg, Germany) in a
211 25µl volume containing 0.5µl of each primer (10µM), 12.5µl of 2x Qiagen Multiplex PCR
212 Master Mix, 9µl of ultrapure water and 2.5µl of extracted DNA. The cycling conditions
213 included an initial denaturation at 95°C (15min) followed by a touchdown on the 10 first
214 cycles of denaturation at 94°C (20s *Tnf* ; 40s *Mx2* and *Tlrs*), annealing at 65–55°C (30s
215 *Tnf* : 45s *Mx2* and *Tlrs*) with one degree less at each cycle, extension at 72°C (60s *Tnf*,
216 45s *Mx2*, 90s *Tlrs*), then 30 cycles of denaturation at 94°C (20s *Tnf* ; 40s *Mx2* and *Tlrs*),
217 annealing at 57°C (30s) for *Tnf* or 55°C (45s) for *Mx2* and *Tlrs* and extension at 72°C
218 (60s *Tnf*, 45s *Mx2*, 90s *Tlrs*), and a final elongation step at 72°C for 10min.
219 The products of all these reactions were electrophoresed on 1.5% agarose gels and
220 visualized by ethidium bromide staining. PCR products were sequenced in both
221 directions by Eurofins MWG Operon (Ebersberg, Germany). Sequences were edited and
222 aligned in BioEdit Sequences Alignment Editor using ClustalW Multiple Alignment (Hall
223 1999). We next used KASP genotyping services from LGC company (Genotyping by
224 Allele-Specific Amplification Cuppen 2007) to genotype all sampled voles at SNPs that
225 were polymorphic in the Swedish samples.
226
227 *RAD tag sequencing*: we chose to develop high throughput sequencing pools of
228 individuals to reduce sequencing efforts and costs (Gautier et al., 2013; Schlötterer,
229 Tobler, Kofler, & Nolte, 2014). Six equimolar pools (from 35 to 37 individuals per
230 locality) were realized after DNA quality control using Nanodrop, 1,5% agarose gel
231 electrophoresis and Qubit® 2.0 Fluorometer (Invitrogen) quantification.

RAD sequencing was performed following the protocol designed by Etter et al. (2011) and modified by Cruaud et al. (2014). Briefly, DNA pools were digested with 8-cutter restriction enzyme *Sbf*I (21 700 sites predicted following the radcounter_v4.xls spreadsheet available from the UK RAD Sequencing Wiki (www.wiki.ed.ac.uk/display/RADSequencing/Home). For each locality, we built four independent libraries to avoid methodological biases. Digested DNA pools were ligated to a modified Illumina P1 adapter containing locality-specific, 5-6 bp long multiplex identifiers (MIDs). All MIDs differed by at least three nucleotides to limit erroneous sample assignment due to sequencing error (Suppl Mat Table S3). The 24 libraries were then pooled and sheared by sonication using S220 ultra-sonicator (Covaris, Inc.). Genomic libraries were size selected for 300–500 bp by agarose gel excision. P2 adapter were then ligated and fragments containing both adapters (P1 and P2) were PCR enriched during 15 cycles. Libraries were sequenced on an Illumina HiSeq 2000 platform (v3 chemistry) using 2x100 bp paired-end sequencing. Illumina sequencing was performed at the GenePool Genomics Facility (University of Edinburgh, UK).

Sequence reads from Illumina runs were demultiplexed and quality filtered using the *process_radtags* program from the Stacks package version 0.99994. Ambiguous MIDs and low quality reads (Phred < 33) were discarded from further analyses. Sequences were trimmed to 85 nucleotides (position 5 to 90 after the MIDs for the reads 1; position 1 to 85 for the reads 2).

Because no reference genome assembly was available for *M. glareolus*, we needed to build a *de novo* RAD assembly. To that end we first assembled reads 1 per sample with the *ustacks* program from the Stacks package and default options, except for i) the minimum depth of coverage required to create a stack (-m option) that was set to 2; ii)

the maximum distance in nucleotides allowed between stacks (-M option) that was set to 3; and iii) the maximum distance allowed to align secondary reads to primary stacks (-N option) that was set to 2. The resulting set loci were then merged into a catalog of loci by the *cstacks* program from the Stacks package run with default options except for the number of mismatches allowed between sample tags to form stacks (-n option) that was set to 2. For each of the obtained read 1 contigs (i.e., RAD loci), we further assembled the associated reads 2 using *CAP3* (Hang & Madan, 1999) ran with default options except for i) the segment pair score cutoff (-i option) that was set to 25; ii) the overlap length cutoff (-o option) that was set to 25; and iii) the overlap similarity score cutoff (-s option) that was set to 400. If a single contig was produced after a first *CAP3* run, this was retained only if it was associated with less than 5% remaining singleton sequences and supported by more than 40 reads. If several contigs were produced, CAP3 was run a second time (using the same options as above) to try to assemble all of them into a single contig which was in this case retained for further analyses. If read 2 contig overlapped with their corresponding read 1 contig, as assessed with the *blastn* program from the BLAST+ v2.2.26 suite (e-value<1e-10 and percentage of identity above 95), both contigs were concatenated. Otherwise, fifteen 'Ns' were inserted between both contigs.

Sequence reads were aligned to this assembly using the programs *aln* and sampe implemented in *bwa* 0.5.9 and ran with default options. The resulting *bam* files were then jointly analysed with the *mpileup* program from the Samtools v0.1.19 suite. We used default options except for the minimum mapping quality for alignment (-q option) that was set to 20. The mpileup file was further processed using a custom awk script to perform SNP calling and derive read counts for each alternative base (after discarding

bases with a Base Alignment Quality score <25) as previously described (Gautier, 2015; Gautier et al., 2013}. A position was considered variable if (i) it had a coverage of >5 and <500 reads in each pool; (ii) only two different bases were observed across all six pools, and (iii) the minor allele was represented by at least one read in two different pool samples. Note that triallelic positions for which the two most frequent alleles satisfied the above criteria with the third allele represented by only one read were included in the analysis as biallelic SNPs (after filtering the third allele as a sequencing error). To prevent any convergence issue with the SELESTIM model-based methods for genome scans that we used (see below), the final dataset was generated by randomizing the reference allele for each and every locus. These procedures were implemented in R (Team 2012) using home-made scripts.

Genetic variation

Diversity at immune-related candidate genes: we performed preliminary analyses on the genotypes inferred at candidate gene SNPs. Observed (H_o) and expected (H_e) heterozygosities as well as F_{IS} were estimated using GENEPOP v4.2 (Rousset 2008). Deviation from Hardy-Weinberg equilibrium was assessed using exact tests implemented in GENEPOP v4.2. Linkage disequilibrium (LD) was estimated using the program LINKDOS implemented in GENETIX V4.05 (Belkhir, Borsa, Chikhi, Raufaste, & Bonhomme, 1996-2004). Significance was assessed using permutation tests.

Characterization of population structure: Population structure analyses were conducted at the population level. We assessed the pattern of differentiation between the six populations pairs (and overall) using the F_{ST} estimator developed by Hivert et al. (in

prep., script available upon request) for poolseq data. Next, we estimated the scaled covariance matrix of population allele frequencies using the algorithm implemented in BAYPASS (Gautier, 2015). A principal component analysis (PCA) was performed on this matrix using the FactomineR library in R (Team 2012) to visualize the patterns of population structure. All SNPs were included, as BAYPASS is likely to be only lightly sensitive to the inclusion of markers evolving under selection when estimating the covariance matrix (Lotterhos & Whitlock, 2014). Finally, we tested for an isolation by distance pattern by analysing the relationship between pairwise genetic distance, estimated as F_{ST} / (1 – F_{ST}), and the logarithm of geographical distance using a Mantel test implemented in R.

Detecting putative footprints of selection based on differentiation

We used two different methods to characterize markers showing outstanding differentiation (as compared to the rest of the genome) between PUUV endemic and non-endemic areas in Sweden. In these analyses, all candidate loci polymorphisms and RAD SNPs were included.

First, we used the software package SELESTIM 1.1.3 , which is based on a diffusion approximation for the distribution of allele frequencies in a subdivided population (island model) that explicitly accounts for selection. In particular, SELESTIM assumes that each and every locus is targeted by selection to some extent, and estimates the strength of locus-specific selection for each locus, in each subpopulation. SELESTIM has been extended since version 1.1.0 to handle Pool-Seq data. Three different SELESTIM analyses were run to assess convergence. For each analysis, twenty-five short pilot runs (1 000 iterations each) were set to adjust the proposal distributions for each model parameter

328 and, after a 100 000 burn-in period, 100 000 updating steps were performed. Samples
329 were collected for all the model parameters every 40 steps (thinning interval), yielding 2
330 500 observations. Convergence was checked using the Gelman–Rubin's diagnostic
331 implemented in the CODA package for R (Plummer, Best, Cowles, & Vines, 2006).
332 Candidate markers under selection were selected on the basis of the distance between
333 the locus-specific coefficient of selection and a "centering distribution" derived from the
334 distribution of a genome-wide parameter of selection, which accounts for the variation
335 among loci of selection strength. SELESTIM uses the Kullback–Leibler divergence (KLD) as
336 a distance between the two distributions, which is calibrated using simulations from a
337 predictive distribution based on the observed data (Vitalis, Gautier, Dawson, &
338 Beaumont, 2014). Hereafter, we report candidate markers with KLD values above the
339 99.9% quantile of the so-obtained empirical distribution of KLD (although the results
340 based on the 99.95 and 99.99 % quantiles are also provided).
341 Next, we used the software package BAYPASS (Gautier, 2015), which extends the
342 approach by Coop et al. (2010) and Günter and Coop (2013). This method relies on the
343 estimation of the (scaled) covariance matrix of population allele frequencies, which is
344 known to be informative about demographic history. Therefore, contrary to SELESTIM,
345 BAYPASS is not limited by the oversimplification of the underlying demographic model.
346 To identify SNPs targeted by selection, we used BAYPASS to estimate the statistic X^TX,
347 which might be interpreted as a locus-specific analog of F_{ST}, explicitly corrected for the
348 scaled covariance of population allele frequencies. To define a significance threshold for
349 the X^TX statistic, we used an empirical posterior checking procedure, similar in essence
350 to the one used in SELESTIM to calibrate the KLD. The posterior predictive distribution of
351 X^TX was obtained under the null (core) model, by generating and analysing a pseudo-

observed dataset (pod) made of 20,000 SNPs (Gautier, 2015). We checked that the scaled covariance matrix of population allele frequencies estimated from the pod was close to the matrix estimated from our data (*FMD* distance = 0.088, see (Gautier, 2015)). The decision criterion for identifying X^TX outliers was defined from the quantiles of the X^TX distribution of the pod analysis.

Detecting putative footprints of selection based on environmental variables

We used BAYPASS to test for associations between allele frequencies and environmental variables presumably related to PUUV epidemiology, while controlling for demography. The STD model in BAYPASS assumes a linear effect of the environmental variable on allele frequencies. We chose empirical Bayesian *P*–values (*eBP*) as the decision criterion, because it was more stable than Bayes Factors (BF) in the sense that estimates were highly correlated across multiple independent runs (see also Bourgeois et al., 2017). Similarly, MCMC sample based estimate of BF (-auxmodel option) or eBP (-covmcmc option) were inaccurate likely due to identifiability issues related to the too small number of populations considered. Roughly speaking, for a given SNP, the empirical Bayesian *P*–value measures to which extent the posterior distribution of the regression coefficient excludes 0 (Gautier, 2015). In order to compute the *eBP*, we used the importance sampling algorithm implemented in BAYPASS to estimate the moments of the posterior distribution of the regression coefficients. We calibrated *eBP* using simulations from a posterior predictive distribution, based on the observed data set.

Environmental variables related to PUUV prevalence in human (number of nephropathia epidemica cases), climate, forest composition and shape, and soil water content, were selected with regard to PUUV ecology in Europe as they should reflect

PUUV distribution in Sweden (Zeimes et al., 2012; Zeimes et al., 2015) (Table 2). Except for the number of nephropathia epidemica cases that was only available per county, variables were computed within an area covering a circular radius of 3 km around each sampling site (ArcGIS 10.1), which is an acceptable estimate of vole dispersal capacity (Le Galliard, Rémy, Ims, & Lambin, 2012). To summarize climate variation, we used the minimum temperature in winter (December, January and February), the maximum temperature in summer (June, July and August), the percentage of the area covered by snow and the annual precipitation. Land-use was characterized by forest types (the proportion in the 3km buffer of forest, coniferous, broadleaved and mixed forest) and by tree species (the volume of spruce and pine and their standard deviation). Forest patches metrics (computed with FRAGSTATS, version 4, http://www.umass.edu/landeco/research/fragstats/fragstats.html) were averaged in the 3km buffer and included the contiguity index, the shape index (a shape index of one represents the most compact shape, upper than one, a more complex shape) and the perimeter. Finally, the soil water index (SWI) representing the soil moisture conditions was also included.

To reduce the dimensionality of these environmental data, we assessed SNP-environment associations using the two first principal components (PC) from a PCA that included all 15 variables (Fig. 2). These new synthetic variables explained respectively 44.1% and 36.6% of the total variance. PC1 represented an environmental, latitudinal gradient. Along this axis, sampling localities were ranked from northern localities (positive values) exhibiting high numbers of human PUUV infection and large volume of spruce forests, to southern localities (negative values) with mixed or broadleaved forests, low mean winter and high maximum summer temperatures. PC2 strongly

400 opposed the two northern sampling localities, with Hörnefors (negative values) being
401 characterized by large volume of contiguous coniferous forest and high snow coverage,
402 and Harnosand (positive values) being more fragmented.
403
404 *Annotations and gene ontology analysis*
405 *Annotation of contig sequences :* We applied several approaches to functionally annotate
406 the contigs. First, all consensus sequences (reads1-reads2) were blasted against the
407 NCBI NT (v. 03/29/2015) and NR (v. 05/16/2015) databases using the blastn (v.
408 2.2.28+, parameters: threshold e-value of 1e-5, minimum alignment percent identity of
409 70%) and blastx (e-value of 1e-5) search algorithms, respectively. In-house Perl scripts
410 were applied to further filter these BLAST results. Only matching sequences of the taxon
411 '*rodentia*' were considered.
412 In addition, in the absence of a published complete genome of *M. glareolus*, we
413 compared the RAD contigs to the genome of *Mus musculus* (build GRCm38/mm10). We
414 downloaded (date: 2015-06-25) the sequences of the 22 mouse chromosomes, 90,891
415 cDNAs and 87,139 proteins from ENSEMBL (http://www.ensembl.org/) and blasted the
416 RAD contigs against these sequences (blastn for genome and cDNA, blastx for proteins
417 with same parameters as mentioned above).
418
419 *Gene enrichment analysis of outlier candidates:* For enrichment analyses of metabolic
420 pathways and Gene Ontologies (GO), we applied the KOBAS web-application (KOBAS
421 2.0, http://kobas.cbi.pku.edu.cn). For this purpose, we extracted the ENSEMBL gene ids
422 from the blastx results of the RAD outliers versus the ENSEMBL protein dataset and also
423 included the gene id of the candidate *Tlr7*. The metabolic pathway databases KEGG,

Reactome, BioCyc and PANTHER, as well as the GO database were chosen for the enrichment analysis. The genome of *Mus musculus* (GRCm38) was chosen as species of interest. On both ENSEMBL id sets the 'annotate' and 'identify' programs of KOBAS were executed with the ENSEMBL ids of the unique set of outliers (all methods combined) as sample file and the ids of the entire GRCm38 coding gene set as background dataset. For these analyses, the other parameters of the 'identify' program were left on default settings. Therefore, the enrichment analysis was done using the hypergeometric and Fisher's exact tests, and Benjamini and Hochberg's method was applied for FDR correction (Benjamini & Hochberg, 1995). A metabolic pathway was considered as significantly enriched, if the associated *q*-value was less than or equal to 0.05. Finally, a full network representation was provided using the Search Tool for the Retrieval of Interacting Genes (STRING) database (Snel, Lehmann, Bork, & Huynen, 2000). Furthermore, we ran the web program REVIGO (web version of 07/27/2015, http://revigo.irb.hr/ ; http://www.ncbi.nlm.nih.gov/pmc/articles/PMC3138752/) to group significantly enriched Gene Ontology (GO) terms into GO categories and to summarise the GO terms to common terms. We applied the SimRel semantic similarity measure with the default GO term similarity, associated *q*-values to the enriched GO terms, and the *Mus musculus* database (Supek, Bošnjak, Škunca, & Šmuc, 2011).

Results

RAD tag sequencing

Sequencing of the 24 RAD libraries (6 localities and 4 replicates) generated 340,692,418 reads, with an average of ca. 13.5 million reads per Multiplex Identifiers (MIDs). The number of sequences generated per locality and MID ranged between ca. 10.1 and ca.

15.1 million reads. After trimming sequences to 85 bp and after filtering for quality, an average of ca. 12.6 million reads per MID (representing 93.5% of the total) were retained. Read 1 assembling produced 151.522 contigs. The first *CAP3* assembling run of the associated reads 2 produced 46474 unique contigs represented by more than 40 sequences, and among which 46.471 had less than 5% singleton. The second *CAP3* assembling run enabled to provide 69.777 read 2 contigs. We found a single significant alignment between read 1 and read 2 contigs in 59.242 cases and no significant overlap in 10.495 cases. The other 38 cases corresponded to a complete alignment of read 1 contig with read 2 contig (1 case), an alignment of read 1 contig within read 2 contig (2 cases) and multiple significant alignment (35 cases). The resulting assembly finally consisted of 69,777 contigs spanning 38.482 Mb (average contig size equal to 551.5, [209-891]).

Reads were aligned to this reference contig dataset and 485,182 SNPs were detected (QC > 25, depth range: 5-500X). Among them 95,988 SNPs distributed on 70,699 contigs were kept according to the more stringent criteria described before.

Descriptive statistics

Candidate gene diversity: The Sanger sequencing of the four immunity-related genes for 12 individuals identified a total of 20 variable sites (19 SNPs and one insertion-deletion event) from 5395 bp sequence data (Suppl. Mat. Table S4). Each gene had between one (*Tlr7*) and 14 (*Tlr4*) SNPs. Eight of these SNPs were polymorph in Sweden and were successfully genotyped in 250 bank voles using the KASP genotyping (Table 3).

Not surprisingly, significant linkage disequilibrium (LD) was observed between most SNPs located within genes: Tlr4-exon3 776 and Tlr4-exon3 1146, Tlr4-exon3 1662,

Tlr4-exon3 1687; Tlr4-exon3 1146 and Tlr4-exon3 1662, Tlr4-exon3 1687; Tlr4-exon3 1662 and Tlr4-exon3 1687. We did not detect any linkage disequilibrium among SNPs located in different genes.

Estimates of diversity indices per SNP and per sampling locality can be found in Table 4. Deviation from Hardy-Weinberg equilibrium was observed in most localities for *Tnf* promoter (-296) with significant deficits in heterozygotes detected in Hörnesand, Harnefors, Njurunda and Gimo. Moreover, significant departures from Hardy-Weinberg expectations were observed in Gimo for all polymorphic SNPs in this locality.

Characterization of population structure: The multilocus F_{ST} between pairs of populations ranged from 0.091 to 0.361, and the overall differentiation among populations was estimated as F_{ST} = 0.212 (Suppl. Mat. Fig. S1). We found a significantly positive correlation between pairwise genetic distance, estimated as F_{ST} / (1 - F_{ST}), and the logarithm of geographical distance (Mantel test; p = 0.0014). The PCA performed on the covariance matrix of population allele frequencies revealed a strong differentiation between the northern populations Hörnefors (mitochondrial lineage 'Ural'), Härnösand (mitochondrial lineage 'western') and all other populations on the first axis. The second axis differentiated the southern population of Gimo from all other populations (Fig. 3a). The scaled covariance matrix of population allele frequencies estimated with BAYPASS was also consistent with a strong differentiation between Hörnefors and Härnösand populations on the one hand, and more southern populations on the other hand (Fig. 3b), as well as with an isolation-by-distance pattern (Fig. 3c).

Signatures of selection

496 *SELESTIM:* The Gelman–Rubin's diagnostic was equal to 1.06 for the hyper-parameter λ,
497 which represents the genome-wide effect of selection over all demes and loci, and to
498 1.11 for the parameters *M*, which represent the scaled migration parameters. This
499 indicates that the chains converge satisfactorily to the target distribution. One replicate
500 analysis was therefore picked at random for the rest of the study. The 99.9% quantile of
501 the posterior predictive distribution of the KLD (based on pseudo-observed data)
502 equalled 2.61. We found a total of 86 SNPs, representing 78 unique contigs and the
503 candidate gene *Tlr7*, with a KLD estimate equal to or larger than this threshold (48 SNPs
504 were identified as outliers using the 99.95% quantile threshold, and 37 at the 99.99%
505 threshold). All these outliers showed high F_{ST} estimates compared with the background
506 F_{ST} (Fig. 4a). We found a clinal pattern of variation for the locus- and population-specific
507 coefficients of selection estimated by SELESTIM along the North / South axis of sampling.
508 Furthermore, we found, for most outliers, that the coefficients of selection were
509 correlated with the first principal components of the environmental variables that
510 discriminate areas of high PUUV prevalence in humans from non-endemic PUUV areas
511 (Fig. 4b).
512
513 *BAYPASS:* Considering the core model implemented in BAYPASS (i.e., the covariable-free
514 approach), we found 10 outlier SNPs, belonging to nine unique contigs (X^TX > 14.88,
515 99.9% quantile). Six SNPs corresponding to five unique contigs were common with the
516 SELESTIM analysis (Fig. 5a). Considering the 99.95% and the 99.99% quantiles we found
517 five and one outlier SNP(s), respectively. Out of these, three (respectively zero) were
518 common with the SELESTIM analysis (Suppl. Mat. Fig. S2).

519 Using the STD model in BAYPASS (which allows the evaluation of associations between
520 SNP allele frequencies and environmental variables), we found 483 SNPs (belonging to
521 413 unique contigs) with strong association signals (*eBP* > 15.35). A total of 395 SNPs –
522 corresponding to 339 unique contigs – showed significant association with the first
523 principal component of the environmental variables, that discriminate areas of high
524 PUUV prevalence in humans from non-endemic PUUV areas (Fig. 5b). Among them, 26
525 contigs were previously detected using SELESTIM only (24 contigs) or SELESTIM and
526 BAYPASS core model (2 contigs). Ninety SNPs – corresponding to 77 unique contigs –
527 were associated with the second principal component of the environmental variables
528 (Fig. 5c). Four of these contigs were previously detected as outliers: three from the
529 BAYPASS STD model with the first PC, and another one from the SELESTIM analysis. None
530 of these SNPs were found as outliers in the BAYPASS core model. Results obtained with
531 other threshold values are provided in Suppl. Mat. Fig. S2.
532
533 *Annotation and gene ontology analysis*
534 *Annotation of contig sequences:* blastn provided an annotation for 49.6% (34,578
535 contigs) of 69,777 bank vole contigs tested across Rodentia databases; blastx led to an
536 annotation for 19.8% (13,830 contigs) of them. In total, the BLAST similarity matches
537 could be assigned to twelve rodent species. The Chinese hamster (37.5%), the house
538 mouse (27.3%) and the Norway rat (17%) were among the most represented rodents.
539 When considering the genome sequence of *M. musculus* obtained from ENSEMBL, we
540 observed that all 22 mouse chromosomes were covered by RAD contigs (*n* = 30,929, i.e.,
541 44.3%). Moreover, about 20% (*n* = 13,856) of the 69,777 bank vole contigs were located
542 in 6,077 mouse protein-coding genes (cDNAs). Out of these, 9,606 (13.8%) bank vole

543 RAD contigs were actually located in the coding sequence of 4,706 mouse proteins (the
544 other RAD contigs were more likely located in UTR termini of the cDNA).
545
546 *Annotation, function and gene enrichment analysis of outlier candidate genes:* Gene
547 enrichment analysis was performed on the 468 bank vole outlier contigs detected by at
548 least one of signature selection methods. Among them, 191 were aligned to the mouse
549 genome, covering 20 mouse chromosomes. In total, 52 outliers – including the *Tlr7*
550 candidate gene – matched to 44 mouse protein-coding genes (Table 5). Note that 10 of
551 these genes were coding for proteins that are involved in immunity (*Dgkd*, *Fermt3,*
552 *Il12rb1, Lbp, Lilrb4, Nedd4, Ptprc, Tlr7, Tnfrsf22, Vwa*). They were either detected by the
553 algorithms of SELESTIM or BAYPASS with environmental associations.
554 The protein-protein interaction network analysis emphasized the importance of
555 immunity pathways within this set of annotated outliers. It described eight edges
556 corresponding to associations between five immune related outliers detected in this
557 study (*Ptprc*, *Tlr7*, *Fermt3*, *Dgkd* and *Lilrb4*). The significance of this network
558 (enrichment *p-value* = 0.001) indicated that the encoded proteins are at least partially
559 biologically connected (Fig. 6).
560 Using Kegg pathway, Reactome, PANTHER and BioCyc databases for pathway
561 annotations, we detected 30 pathways with significant enrichment ($p < 0.05$, Table 5).
562 Four of them were linked to TLR pathways, for which we had strong *a priori* reasons to
563 believe that they were involved in adaptive divergence. Seven other significantly
564 enriched pathways were directly related to immunity ('Antiviral mechanism by IFN-
565 stimulated genes'; 'Antigen activates B Cell Receptor'; 'Platelet calcium homeostasis';
566 'citrulline biosynthesis'; 'ISG15 antiviral mechanism') or indirectly ('Elevation of

567 cytosolic Ca2+ levels'; 'Choline metabolism in cancer'). Another interesting pathway
568 with regard to bank vole / PUUV interactions was 'Surfactant metabolism', since some of
569 the proteins involved in this pathway can interact with pulmonary viral infections. All
570 outliers involved in these enriched pathways were detected using the STD model in
571 BAYPASS, except *Tlr7* that was also detected using SELESTIM. Finally, other important
572 classes of enriched pathway categories were related to metabolism, in particular fatty
573 acid metabolism, and neurotransmission.

574 Among the gene-associated GO terms, 210 had *p*-values below 0.05. Of these GO
575 terms, 176 belonged to the GO category Biological process, 21 to Molecular Function and
576 13 to Cellular Component. REVIGO formed nine clusters for the category Biological
577 Process (Fig. 7). The most represented cluster was built by the term 'positive regulation
578 of chemokine production', followed by 'substrate adhesion-dependent cell spreading',
579 'myeloid leukocyte activation' and 'secretion of lysosomal enzymes'. For the GO category
580 'Molecular Function' nine GO term clusters were formed among which the most common
581 terms comprised 'beta-galacoside (CMP) alpha-2,3-sialyltransferase activity', 'Wnt-
582 activated receptor activity', 'phosphoserine binding' and 'lipoteichoic acid binding'.
583 Finally, the GO terms 'receptor complex' and 'sarcoplasmic reticulum membrane'
584 summarised the clusters of the Cellular Component category.

585

586 **Discussion**

587 *A new toolbox for Myodes glareolus studies*

588 Recent years have seen the advent of high throughput sequencing and genotyping
589 technologies and their application to non-model organisms. It has opened new
590 perspectives to perform genomic studies and identify genes and networks involved in a

591 diverse array of ecological and evolutionary processes including speciation,
592 conservation, invasion or biological adaptation (Andrews, Good, Miller, Luikart, &
593 Hohenlohe, 2016; Ekblom & Galindo, 2011; Narum, Buerkle, Davey, Miller, & Hohenlohe,
594 2013). In the context of zoonoses, these technologies have mostly been used to study
595 newly emerging pathogens (Yang, Yang, Zhou, & Zhao, 2008). The analysis of gene
596 interactions that govern host or reservoir responses to pathogens still remains mostly
597 restricted to laboratory models and major diseases (e.g. malaria vectors, White et al.,
598 2011). In this study, we used paired-end RAD sequencing to examine the genomic
599 patterns of differentiation among six natural populations of *Myodes glareolus,* a rodent
600 reservoir of *Puumala* virus, the agent of a mild hemorrhagic fever with renal syndrom in
601 humans. This study complements previous ones that focused on candidate genes
602 selected from the literature to identify those involved in bank vole susceptibility to
603 PUUV (Charbonnel et al., 2014). It also provides genomic resources of tens of thousands
604 RAD-seq markers that will further be available to study genetic diversity, population
605 structure and adaptation in bank voles. They may be very useful to address different
606 issues related to this rodent in a wide array of disciplines such as medical science
607 (Hampton, 2014; Razzauti-Feliu et al., 2015), microbiology (Kohl, Sadowska, Rudolf,
608 Dearing, & Koteja, 2016), or ecology (Mokkonen et al., 2011).
609
610 *High levels of genetic differentiation between northern and southern bank voles*
611 These genomic data provide population structure patterns that are in agreement with
612 the previous phylogeographic studies conducted on bank voles based on mitochondrial
613 sequences and mitogenomes. The stronger level of differentiation was observed
614 between the northernmost population (Hörnefors) and the southern ones (pairwise F_{ST}

615 comprised between 0.248 and 0.361), in line with a strong pattern of isolation by
616 distance. This result is also congruent with the macrogeographic pattern classically
617 observed in Fennoscandia, where two main differentiated mitochondrial lineages are
618 present respectively in Southern and North-Eastern Sweden (Jaarola, Tegelstrom, &
619 Fredga, 1999; Tegelstrom & Jaarola, 1998). The recolonization of Fennoscandia, from
620 separate glacial refugia, after the end of the last glaciation period, shaped this
621 phylogeographic pattern, with a southern immigration route that became accessible
622 around 14,1000 BP and a north-eastern one that opened up 10,000 BP (Jaarola et al.,
623 1999). It created a ca. 50 km-wide secondary contact zone between these two
624 mitochondrial lineages, which runs from West to East through Central Sweden, between
625 Hörnefors and Härnösand localities. The genome-wide differentiation observed in this
626 study reflects this phylogeographic history. This contact zone is also detected for other
627 mammalian species including the common shrew, the brown bear and the field voles
628 (Taberlet & Bouvet, 1994). Such suture zone cannot be explained by past or present
629 natural barriers to dispersal (Jaarola et al., 1999), but rather by a secondary contact
630 between divergent recolonizing lineages. Secondary contact might result from similar
631 phylogeographic histories for different mammalian species, or analogous selective
632 pressures acting on these species. Interestingly, Puumala viruses circulate on both sides
633 of this contact zone, with distinct genetic variants in the northern and in the southern
634 bank vole populations, which suggests that a contact zone may also exist between
635 genetically differentiated PUUV lineages (Hörling et al., 1996).
636
637 *Biological limitations*
638
639 Because of the phylogeographical history of *M. glareolus* in Sweden, the transect

between the PUUV endemic (Northern Sweden) and non-endemic (Southern Sweden) areas included a contact zone between two genetically differentiated bank vole lineages. Our sampling was therefore marked by a strong genetic structure, that coincided spatially with gradients in ecological variables as well as PUUV distribution.

A first consequence is the possibility that F_{ST} outliers do not result from local adaptation but from genetic incompatibilities between different backgrounds. Such endogeneous genetic barriers may result in tension zones, whose locations are initially stochastic but tend to overlap with exogenous ecological barriers (coupling effect, see Bierne, Welch, Loire, Bonhomme, & David, 2011). It is nearly impossible to disentangle F_{ST} outliers from genetic incompatibilities in our case, but replicating this work along other PUUV endemic – non-endemic transects could help identifying loci commonly evolving in response to PUUV in bank vole populations.

A second consequence of this sampling strategy concerns the lack of statistical power to detect local adaptation while using F_{ST} outlier statistical methods. These methods are often based on theoretical assumptions (e.g., populations at equilibrium, island model of migration) that are rarely completely met in the natural populations sampled. Moreover, spatial autocorrelations in allele frequencies due to isolation by distance can result in false correlations between such frequencies and environmental variables (Lotterhos & Whitlock, 2015; Meirmans, 2012). This potential effect may result in a larger number of false positive detected with SELESTIM (which assumes an island model of population structure) as compared to BAYPASS, and a low number of common outliers between SELESTIM and BAYPASS. This justified the use of genetic-environment associations statistical methods controlling for population structure (here, BAYPASS). However, this method may also have low statistical power with our sampling design due to the strong

664 correlation between the axis of population genetic differentiation (North-South isolation
665 by distance pattern) and the axis of environmental variations (including variations in
666 PUUV prevalence). Unfortunately, it was not possible to study pairs of nearby
667 populations, as recommended by Lotterhos et al. (2015), because the limit between
668 geographic areas where PUUV pressure is high vs. low is barely known. We therefore
669 had to consider a large sampling scale for bank vole populations, which led to highly
670 genetically structured samples. Finally, it is likely that little information about
671 divergence and selection came from the populations sampled in the middle of the
672 transect, where PUUV pressure as well as environmental and climatic features were
673 intermediate. Future studies should now focus on samples covering the geographic area
674 where clines of allele frequencies exhibit slope disruption.

675 Because of these biological limitations, genome scan results have to be considered
676 cautiously. The combination of three statistical analyses based on population
677 differentiation and ecological associations to detect outlier loci aimed to reduce the rate
678 of false positives and to enhance our chances of detecting genuine signatures of
679 selection (François, Martins, Caye, & Schoville, 2016). The enrichment tests and gene
680 interaction network analyses may also limit interpretations of false positive outliers.

681

682 *Genes involved in selection*

683 We found evidence for a small set of outlier loci (547 SNPs belonging to 468 contigs
684 among 70,699 examined), showing high levels of genetic differentiation consistent with
685 divergent selection acting along our North-South transect in Sweden. Because the whole
686 genome of *Myodes glareolus* is not yet sequenced, assembled and annotated, we met
687 difficulties in annotating RAD contigs and consequently, outlier ones**.** Only 41 % of the

688 outlier contigs blasted to genes in the mouse genome. Among them, only 21 % belonged
689 to protein coding regions and could be annotated. We therefore could only work on a
690 small part of the information gathered. Moreover we have to remind that this genome
691 scan approach enabled to screen about 35 Mbp, *i.e.* about 1 % of the genome bank vole.
692 Altogether, these facts may explain why this population genomic approach could hardly
693 reveal previously identified candidate genes with regard to bank vole susceptibility to
694 PUUV (Charbonnel et al., 2014). Despite these limits, we have succeeded in identifying
695 other genes and pathways probably evolving under differential selection among bank
696 vole populations from PUUV endemic and non-endemic areas. One third of the enriched
697 pathways representing SNPs showing these signatures of directional selection
698 concerned immune processes, with the 'positive regulation of chemokine production'
699 being among the most represented biological process. Infectious pathogens are among
700 the strongest selective forces acting in natural populations, and as such, they contribute
701 to shape patterns of population divergence and local adaptations in the wild through
702 balancing and positive selection acting in host genomes (e.g. Fumagalli et al., 2011;
703 Karlsson et al., 2014; Vatsiou, Bazin, & Gaggiotti, 2016). Many of the immune related
704 genes showing footprint of positive selection here were detected using ecological
705 associations with a synthethic variable describing North / South variations in climatic,
706 forest features and nephropatia epidemica human cases. Although these associations do
707 not reflect causality, they might be biologically meaningful with regard to environmental
708 factors and *M. glareolus* microbiome, including PUUV, that influence bank vole responses
709 to parasitism and genetic polymorphism. Further analyses and experiments are
710 required to confirm and better interpret this result.

More specifically, the analysis of gene interaction network provided support in favor of this potential local adaptation to environment for molecules involved in platelet activation (*Fermt3*, *Dgkd*) and TLR pathway (*Tlr7*). The pattern recognition receptors (PRR) for hantaviruses include Toll-Like receptors, among which TLR7. Its stimulation activates downstream signalling immune cascades with production of pro-inflammatory cytokines and IFNs, which are crucial for inducing a variety of innate antiviral effector mechanisms (Kawai & Akira, 2005). Differential genetic expression of this receptor or different levels of TLR7-Hantavirus recognition due to TLR7 genetic polymorphism could affect this activation of immune cascade, with consequences in terms of virus replication (e.g. for Tlr7 gene expression between sexes, Klein et al., 2004). Moreover, in humans, hantavirus-associated syndromes include increased vascular permeability and platelet dysfunction, with dramatic decreases in platelet counts at the beginning of vascular leakage (Yanagihara & Silverman, 1990). The presence of functional platelet-TLR7 and their activation during viral infections could result in this decrease of viral platelet count, which is likely due to platelet aggregate formation with leukocytes, followed by internalization in the neutrophil population (Koupenova et al., 2014). In addition, hantaviruses bind to $\alpha_{IIb}\beta_3$ integrins expressed on platelets and endothelial cells, contributing to viral dissemination, platelet activation, and induction of endothelial cell functions. Gavrilovskaya et al. (2010) suggested that hantavirus associated pathogenesis could be due to the recruitment of quiescent platelets to the surface of infected endothelial cells, thereby forming a platelet covering on the surface of the endothelium. This could dramatically reduce the number of circulating platelets and alter platelet and endothelial cell interactions, which dynamically regulate vascular integrity. In reservoirs, hantaviruses persist without exhibiting any sign of immune pathology and

735 they evade immune responses to establish persistence (Easterbrook & Klein, 2008).
736 Deer mice infected with SNV or ANDV did not show any variations of platelet counts
737 compared to uninfected one {Schountz, 2012 #1409}. Our results might therefore
738 suggest that genetic polymorphisms associated with *Tlr7* or platelet activation genes
739 may account for differences in the immune responses to PUUV infections, and the
740 possibility for this virus to persist in *M. glareolus*. These polymorphisms could
741 contribute to shape the contrasted PUUV epidemiological situations observed in natural
742 populations of bank voles from Northern and Southern Sweden.

743 In addition, several genes encoding molecules with functions in metabolic processes
744 related to glycolysis / glucogenesis, lipid metabolism and citric acid cycles, showed
745 signatures of selection that were mainly detected from ecological associations with the
746 synthethic variable describing North / South variations in Sweden. Previous studies
747 have demonstrated that energy metabolism shows important inter- and intraspecific
748 variations in endotherms driven by physiological, ecological and evolutionary factors
749 (Boratynski et al., 2011). It is likely that the rate of metabolism is correlated with life
750 history traits and fitness components , although different correlations can be observed
751 due to fluctuating selection between seasons (Nilsson & Nilsson, 2016). We can
752 therefore speculate that polymorphism at these genes (*Acsbg1, Atp4a, Chpt1, Eno1,*
753 *Hmgn2, Itpr2, Nuak2, Ocrl, Prodh2, St3gal2, Zfp113*, see Table 5) might contribute to
754 bank vole local adaptation to climatic and ecological conditions along a North / South
755 transect accross Sweden. Previous studies based on globin genes in bank voles from
756 Britain found similar patterns of genetic divergence between northern and southern
757 populations, mediated by natural selection through the evolution of bank vole
758 erythrocyte resistance to oxidative stress (Kotlik et al., 2006).

759

760 *Methodological considerations*

761 RAD-seq has become an increasingly common genome scan approach this last decade,
762 although several difficulties regarding the identification of genes of functional
763 significance with regard to population divergence and local adaptations have been
764 pointed out (Lowry et al., 2017). Some of these potential limitations are discussed
765 below.

766 First, we chose to develop a RAD-seq approach based on the pooling of samples
767 without individual barcoding, so that we could estimate population allele frequencies at
768 an affordable cost. Nevertheless, there are several limitations to pooling strategies
769 (Gautier et al., 2013; Narum et al., 2013). Uneven sequencing of individuals in pools may
770 lead to biases in allele frequency estimates. As recommended in Andrews et al. (2016) or
771 Guo et al. (2016), we minimized this bias by including large sample size per pool and
772 replicating libraries for each population. Another possible shortcoming of pooling is that
773 cryptic population structure cannot be identified and taken into account in the case
774 where multiple independent groups of individuals are mixed within a single pool. This
775 possibility was minimized by sampling bank voles in a limited geographic area for each
776 population, although we cannot discard the possibility of intra-population structuring,
777 which is frequent in rodents.

778 Second, we are aware that the RAD-seq approach enabled to sample only a small
779 proportion of *M. glareolus* genome so that we might have missed potentially important
780 adaptive SNPs (Lowry et al., 2017). This limitation was reinforced by the lack of genomic
781 resources for bank voles, that prevent us from identifying a large part of outlier SNPs.
782 Nevertheless, we think that RAD-seq was the most appropriate approach for bank vole

783 population genomics considering the large genome size of this species, the absence of
784 genome reference and the number of individuals and populations we had to screen
785 (McKinney, Larson, Seeb, & Seeb, 2016).
786
787 *Conclusions*
788 Using a pool RAD-seq approch and a combination of statistical methods to detect loci
789 with high genetic differentiation and associations with environmental variables of
790 interests, we have identified a list of putative loci that are worthy for further
791 experimental and functional studies to better understand *Myodes glareolus* / PUUV
792 interactions, and potentially NE epidemiology. These results are of main importance
793 because our previous knowledge of the factors driving immuno-heterogeneity among
794 reservoirs of hantaviruses was inferred from the medical literature or from results
795 based on laboratory models. In the future, they could enable to better assess the risk of
796 NE emergence by including reservoir immunogenetics in ecological niche modelling.
797 They could also have important implications for medical purposes, by revealing
798 potential immune and metabolic pathways driving hantavirus pathogenesis in humans
799 and non-reservoirs.
800
801 **Acknowledgments**
802 The authors wish to thank Hélène Holota from TAGC facility for the Covaris sonication of
803 the RAD libraries. Data used in this work were partly produced through the genotyping
804 and sequencing facilities of ISEM (Institut des Sciences de l'Evolution-Montpellier) and
805 Labex Centre Méditerranéen Environnement Biodiversité. This article is registered with
806 the EDENext Steering Committee as EDENext406 (http://www.edenext.eu/).

807

808 **References**

809 Andrews, K. R., Good, J. M., Miller, M. R., Luikart, G., & Hohenlohe, P. A. (2016).
810 Harnessing the power of RADseq for ecological and evolutionary genomics.
811 *Nature Reviews Genetics, 17*, 81-92. doi:10.1038/nrg.2015.28

812 Baird, N. A., Etter, P. D., Atwood, T. S., Currey, M. C., Shiver, A. L., Lewis, Z. A., . . . Johnson,
813 E. A. (2008). Rapid SNP discovery and genetic mapping using sequenced RAD
814 markers. *Plos One, 3*. doi:10.1371/journal.pone.0003376

815 Barreiro, L. B., & Quintana-Murci, L. (2010). From evolutionary genetics to human
816 immunology: how selection shapes host defence genes. *Nature Reviews Genetics,*
817 *11*, 17-30. doi:10.1038/nrg2698

818 Belkhir, K., Borsa, P., Chikhi, L., Raufaste, N., & Bonhomme, F. (1996-2004). GENETIX
819 4.05, logiciel sous Windows TM pour la génétique des populations. Montpellier
820 (France): Laboratoire Génome, Populations, Interactions, CNRS UMR 5171,
821 Université de Montpellier II.

822 Benjamini, Y., & Hochberg, Y. (1995). Controlling the false discovery rate: a practical and
823 powerful approach to multiple testing. *Journal of the Royal Statistical Society:*
824 *Series B, 57*, 289-300. doi:10.2307/2346101

825 Bierne, N., Welch, J., Loire, E., Bonhomme, F., & David, P. (2011). The coupling
826 hypothesis: why genome scans may fail to map local adaptation genes. *Molecular*
827 *Ecology, 20*, 2044-2072. doi:10.1111/j.1365-294X.2011.05080.x

828 Boratynski, Z., Alves, P. C., Berto, S., Koskela, E., Mappes, T., & Melo-Ferreira, J. (2011).
829 Introgression of mitochondrial DNA among *Myodes* voles: consequences for
830 energetics? *Bmc Evolutionary Biology, 11*. doi:10.1186/1471-2148-11-355

831 Bourgeois, Y. X. C., Delahaie, B., Gautier, M., Lhuillier, E., Male, P. J. G., Bertrand, J. A. M., . . .
832 Thebaud, C. (2017). A novel locus on chromosome 1 underlies the evolution of a
833 melanic plumage polymorphism in a wild songbird. *Royal Society Open Science, 4*.
834 doi:10.1098/rsos.160805
835 Brummer-Korvenkotio, M., Henttonen, H., & Vaheri, A. (1982). Hemorrhagic fever with
836 renal syndrome in Finland: Ecology and virology of Nephropathia Epidemica.
837 *Scandinavian Journal of Infectious Diseases, 36*, 88-89.
838 Charbonnel, N., & Cosson, J. F. (2011). Molecular epidemiology of disease resistance
839 genes with perspectives for researches on biological invasions and hybrid zones.
840 In S. Morand, F. Beaudeau, J. Cabaret, & J. de Rycke (Eds.), *New frontiers of*
841 *Molecular Epidemiology of Infectious Diseases*: Springer.
842 Charbonnel, N., Pagès, M., Sironen, T., Henttonen, H., Vapalahti, O., Mustonen, J., & Vaheri,
843 A. (2014). Immunogenetic factors affecting susceptibility of humans and rodents
844 to hantaviruses and the clinical course of hantaviral disease in humans. *Viruses, 6*,
845 2214-2241. doi:10.3390/v6052214
846 Coop, G., Witonsky, D., Di Rienzo, A., & Pritchard, J. K. (2010). Using environmental
847 correlations to identify loci underlying local adaptation. *Genetics, 185*, 1411-1423.
848 doi:10.1534/genetics.110.114819
849 Cruaud, A., Gautier, M., Galan, M., Foucaud, J., Saune, L., Genson, G., . . . Rasplus, J. Y.
850 (2014). Empirical assessment of RAD sequencing for interspecific phylogeny.
851 *Molecular Biology and Evolution, 31*, 1272-1274. doi:10.1093/molbev/msu063
852 Dubois, A., Castel, G., Murri, S., Pulido, C., Pons, J. B., Benoit, L., . . . Marianneau, P. (2017).
853 Experimental infections of wild bank voles (*Myodes glareolus*) from Nephropatia
854 Epidemica endemic and non-endemic regions revealed slight differences in

855 Puumala virological course and immunological responses. *Virus Research, 235*,
856 67-72. doi:10.1016/j.virusres.2017.04.004
857 Dubois, A., Galan, M., Guivier, E., Henttonen, H., Voutilainen, L., Razzauti, M., . . .
858 Charbonnel, N. (2017). Microevolution of bank voles (*Myodes glareolus*) at
859 neutral and immune related genes during a multi-annual complete dynamic cycle
860 : consequences for Puumala hantavirus epidemiology. *Infection Genetics*
861 *Evolution, 49*, 318–329. doi:10.1016/j.meegid.2016.12.007
862 Easterbrook, J. D., & Klein, S. L. (2008). Immunological mechanisms mediating
863 hantavirus persistence in rodent reservoirs. *Plos Pathogens, 4*.
864 doi:10.1371/journal.ppat.1000172
865 Ekblom, R., & Galindo, J. (2011). Applications of next generation sequencing in molecular
866 ecology of non-model organisms. *Heredity, 107*, 1-15. doi:10.1038/hdy.2010.152
867 Etter, P. D., Preston, J. L., Bassham, S., Cresko, W. A., & Johnson, E. A. (2011). Local de
868 novo assembly of RAD paired-end contigs using short sequencing reads. *Plos One,*
869 *6*, e18561. doi:10.1371/journal.pone.0018561
870 François, O., Martins, H., Caye, K., & Schoville, S. D. (2016). Controlling false discoveries
871 in genome scans for selection. *Molecular Ecology, 25*, 454–469.
872 doi:10.1111/mec.13513
873 Fumagalli, M., Sironi, M., Pozzoli, U., Ferrer-Admetlla, A., Pattini, L., & Nielsen, R. (2011).
874 Signatures of environmental genetic adaptation pinpoint pathogens as the main
875 selective pressure through human evolution. *PLos Genetics, 7*, e1002355.
876 doi:10.1371/journal.pgen.1002355

877 Gautier, M. (2015). Genome-wide scan for adaptive divergence and association with
878 population-specific covariates. *Genetics, 201*, 1555-1579.
879 doi:10.1534/genetics.115.181453
880 Gautier, M., Foucaud, J., Gharbi, K., Cezard, T., Galan, M., Loiseau, A., . . . Estoup, A. (2013).
881 Estimation of population allele frequencies from next-generation sequencing
882 data: pool-versus individual-based genotyping. *Molecular Ecology, 22*, 3766-3779.
883 doi:10.1111/mec.12360
884 Gavrilovskaya, I. N., Gorbunova, E. E., & Mackow, E. R. (2010). Pathogenic hantaviruses
885 direct the adherence of quiescent platelets to infected endothelial cells. *Journal of*
886 *virology, 84*. doi:10.1128/JVI.02405-09
887 Guivier, E., Galan, M., Henttonen, H., Cosson, J. F., & Charbonnel, N. (2014). Landscape
888 features and helminth co-infection shape bank vole immunoheterogeneity, with
889 consequences for Puumala virus epidemiology. *Heredity, 112*, 274-281.
890 doi:10.1038/hdy.2013.103
891 Guivier, E., Galan, M., Ribas Salvador, A., Xuéreb, A., Chaval, Y., Olsson, G., . . . Charbonnel,
892 N. (2010). *Tnf-α* expression and promoter sequences reflect the balance of
893 tolerance/resistance to *Puumala virus* infection in European bank vole
894 populations. *Infection Genetics Evolution, 10*, 1208-1217.
895 doi:10.1016/j.meegid.2010.07.022
896 Gunther, T., & Coop, G. (2013). Robust identification of local adaptation from allele
897 frequencies. *Genetics, 195*, 205-220. doi:10.1534/genetics.113.152462
898 Guo, B. C., Li, Z. T., & Merila, J. (2016). Population genomic evidence for adaptive
899 differentiation in the Baltic Sea herring. *Molecular Ecology, 25*, 2833-2852.
900 doi:10.1111/mec.13657

Hampton, T. (2014). Bank vole a novel model of prion transmission. *Jama-Journal of the American Medical Association, 311*, 1722-1722. doi:10.1001/jama.2014.4334

Hang, X., & Madan, A. (1999). CAP3: A DNA sequence assembly program. *Genome Research, 9*, 868-877. doi:10.1101/gr.9.9.868

Hardestam, J., Karlsson, M., Falk, K. I., Olsson, G., Klingström, J., & Lundkvist, A. (2008). Puumala hantavirus excretion kinetics in bank voles (*Myodes glareolus*). *Emerging Infectious Diseases, 14*, 1209-1215. doi:10.3201/eid1408.080221

Hill, A. V., Allsopp, C. E., Kwiatkowski, D., Anstey, N. M., Twumasi, P., Rowe, P. A., . . . Greenwood, B. M. (1994). Common west African HLA antigens are associated with protection from severe malaria. *Nature, 352*, 595–600. doi:10.1038/352595a0

Hörling, J., Lundkvist, A., Jaarola, M., Plyusnin, A., Tegelström, H., Persson, K., . . . Niklasson, B. (1996). Distribution and genetic heterogeneity of Puumala virus in Sweden. *Journal of General Virology, 77*, 2555-2562. doi:10.1099/0022-1317-77-10-2555

Jaarola, M., Tegelstrom, H., & Fredga, K. (1999). Colonization history in Fennoscandian rodents. *Biological journal of the Linnean society, 68*, 113-127. doi:10.1111/j.1095-8312.1999.tb01161.x

Johansson, P., Olsson, G. E., Low, H. T., Bucht, G., Ahlm, C., Juto, P., & Elgh, F. (2008). Puumala hantavirus genetic variability in an endemic region (Northern Sweden). *Infection Genetics and Evolution, 8*, 286-296. doi:10.1016/j.meegid.2008.01.003

Kallio, E. R., Klingström, J., Gustafsson, E., Manni, T., Vaheri, A., Henttonen, H., . . . Lundkvist, A. (2006). Prolonged survival of Puumala hantavirus outside the host:

924 evidence for indirect transmission via the environment. *Journal of General*
925 *Virology, 87*, 2127-2134. doi:10.1099/vir.0.81643-0
926 Karlsson, E. K., Kwiatkowski, D. P., & Sabeti, P. C. (2014). Natural selection and infectious
927 disease in human populations. *Nature Reviews Genetics, 15*, 379-393.
928 doi:10.1038/nrg3734
929 Kawai, T., & Akira, S. (2005). Pathogen recognition with Toll-like receptors. *Current*
930 *Opinion in Immunology, 17*, 338-344. doi:10.1016/j.coi.2005.02.007
931 Klein, S. L., Cernetich, A., Hilmer, S., Hoffman, E. P., Scott, A. L., & Glass, G. E. (2004).
932 Differential expression of immunoregulatory genes in male and female Norway
933 rats following infection with Seoul virus. *Journal of Medical Virology, 74*, 180-190.
934 doi:10.1002/jmv.20163
935 Kohl, K. D., Sadowska, E. T., Rudolf, A. M., Dearing, M. D., & Koteja, P. (2016).
936 Experimental Evolution on a Wild Mammal Species Results in Modifications of
937 Gut Microbial Communities. *Frontiers in Microbiology, 7*.
938 doi:10.3389/fmicb.7016.00634
939 Kotlik, P., Deffontaine, V., Mascheretti, S., Zima, J., Michaux, J. R., & Searle, J. B. (2006). A
940 northern glacial refugium for bank voles (*Clethrionomys glareolus*). *Proceedings of*
941 *the National Academy of Sciences USA, 103*, 14860-14864. doi:
942 10.1073/pnas.0603237103
943 Koupenova, M., Vitseva, O., MacKay, C. R., Beaulieu, L. M., Benjamin, E. J., Mick, E., . . .
944 Freedman, J. E. (2014). Platelet-TLR7 mediates host survival and platelet count
945 during viral infection in the absence of platelet-dependent thrombosis. *Blood,*
946 *124*, 791-802. doi:10.1182/blood-2013-11-536003

947 Le Galliard, J. F., Rémy, A., Ims, R. A., & Lambin, X. (2012). Patterns and processes of
948 dispersal behaviour in arvicoline rodents. *Molecular Ecology, 21*, 505-523.
949 doi:10.1111/j.1365-294X.2011.05410.x
950 Lotterhos, K. E., & Whitlock, M. C. (2014). Evaluation of demographic history and neutral
951 parameterization on the performance of FST outlier tests. *Molecular Ecology, 23*,
952 2178-2192. doi:10.1111/mec.12725
953 Lotterhos, K. E., & Whitlock, M. C. (2015). The relative power of genome scans to detect
954 local adaptation depends on sampling design and statistical method. *Molecular*
955 *Ecology, 24*, 1031-1046. doi:10.1111/mec.13100
956 Lowry, D. B., Hoban, S., Kelley, J. L., Lotterhos, K. E., Reed, L. K., Antolin, M. F., & Storfer, A.
957 (2017). Breaking RAD: an evaluation of the utility of restriction site-associated
958 DNA sequencing for genome scans of adaptation. *Molecular Ecology Resources, 17*,
959 142-152. doi:10.1111/1755-0998.12635
960 McKinney, G. J., Larson, W. A., Seeb, L. W., & Seeb, J. E. (2016). RADseq provides
961 unprecedented insights into molecular ecology and evolutionary genetics:
962 comment on Breaking RAD by Lowry et al. (2016). *Molecular Ecology Resources*.
963 doi:10.1111/1755-0998.12649
964 Meirmans, P. G. (2012). The trouble with isolation by distance. *Molecular Ecology, 21*,
965 2839-2846. doi:10.1111/j.1365-294X.2012.05578.x
966 Mokkonen, M., Kokko, H., Koskela, E., Lehtonen, J., Mappes, T., Martiskainen, H., & Mills, S.
967 C. (2011). Negative frequency-dependent selection of sexually antagonistic alleles
968 in *Myodes glareolus*. *Science, 334*, 972-974. doi:10.1126/science.1208708

969 Narum, S. R., Buerkle, C. A., Davey, J. W., Miller, M. R., & Hohenlohe, P. A. (2013).
970 Genotyping-by-sequencing in ecological and conservation genomics. *Molecular*
971 *Ecology, 22*, 2841-2847. doi:10.1111/mec.12350
972 Nemirov, K., Leirs, H., Lundkvist, A., & Olsson, G. E. (2010). Puumala hantavirus and
973 *Myodes glareolus* in northern Europe: no evidence of co-divergence between
974 genetic lineages of virus and host. *Journal of General Virology, 91*, 1262-1274.
975 doi:10.1099/vir.0.016618-0
976 Niklasson, B., & LeDuc, J. (1987). Epidemiology of nephropathia epidemica in Sweden.
977 *Journal of Infectious Diseases, 155*, 269-276. doi:10.1093/infdis/155.2.269
978 Nilsson, J. F., & Nilsson, J. A. (2016). Fluctuating selection on basal metabolic rate.
979 *Ecology and evolution, 6*, 1197-1202. doi:10.1002/ece3.1954
980 Olsson, G. E., Leirs, H., & Henttonen, H. (2010). Hantaviruses and their hosts in Europe:
981 Reservoirs here and there, but not everywhere? *Vector-Borne and Zoonotic*
982 *Diseases, 10*, 549-561. doi:10.1089/vbz.2009.0138
983 Petterson, L., Boman, J., Juto, P., Evander, M., & Ahlm, C. (2008). Outbreak of Puumala
984 virus infection, Sweden. *Emerging Infectious Diseases, 14*, 808-810.
985 doi:10.3201/eid1405.071124
986 Plummer, M., Best, N., Cowles, K., & Vines, K. (2006). CODA: Convergence diagnosis and
987 output analysis for MCMC. *R News, 6*, 7-11.
988 Quintana-Murci, L., & Clark, A. G. (2013). Population genetic tools for dissecting innate
989 immunity in humans. *Nature Reviews Immunology, 13*, 280-293.
990 doi:10.1038/nri3421
991 Razzauti-Feliu, M., Galan, M., Bernard, M., Maman, S., Klopp, C., Charbonnel, N., . . .
992 Cosson, J. F. (2015). Comparison of next-generation sequencing approaches

993 surveying bacterial pathogens in wildlife. *Plos Neglected Tropical Diseases, 9*,
994 e0003929. doi:10.1371/journal.pntd.0003929
995 Rohfritsch, A., Guivier, E., Galan, M., Chaval, Y., & Charbonnel, N. (2013). Apport de
996 l'immunogénétique à la compréhension des interactions entre le campagnol
997 roussâtre *Myodes glareolus* et l'hantavirus Puumala. *Bulletin de l'académie*
998 *vétérinaire de France, 166*, 165-176. doi:10.4267/2042/51622
999 Sauvage, F., Langlais, M., Yoccoz, N. G., & Pontier, D. (2003). Modelling hantavirus in
1000 fluctuating populations of bank voles: the role of indirect transmission on virus
1001 persistence. *Journal of Animal Ecology, 72*, 1-13. doi:10.1046/j.1365-
1002 2656.2003.00675.x
1003 Schlötterer, C., Tobler, R., Kofler, R., & Nolte, V. (2014). Sequencing pools of individuals
1004 — mining genome-wide polymorphism data without big funding. *Nature Review*
1005 *Genetics, 15*, 749–763. doi:10.1038/nrg3803
1006 Schmid-Hempel, P. (2003). Variation in immune defence as a question of evolutionary
1007 ecology. *Proceedings of the Royal Society of London, B, 270*, 357-366.
1008 doi:10.1098/rspb.2002.2265
1009 Schulenburg, H., Kurtz, J., Moret, Y., & Siva-Jothy, M. T. (2009). Introduction. Ecological
1010 immunology. *Philosophical transactions of the Royal Society of London, B, 364*, 3-
1011 14. doi:10.1098/rstb.2008.0249
1012 Sheldon, B. C., & Verhulst, S. (1996). Ecological immunology: costly parasite defences
1013 and trade-offs in evolutionary ecology. *Trends in Ecology and Evolution, 11*, 317-
1014 321. doi:10.1016/0169-5347(96)10039-2

1015 Snel, B., Lehmann, G., Bork, P., & Huynen, M. A. (2000). STRING: a web-server to retrieve
1016 and display the repeatedly occurring neighbourhood of a gene. *Nucleic Acids*
1017 *Research, 28*, 3442-3444. doi:10.1093/nar/28.18.3442
1018 Stenseth, N. C. (1985). Geographic distribution of *Chletrionomys* species. *Annales*
1019 *Zoologici Fennici, 22*, 215-219.
1020 Supek, F., Bošnjak, M., Škunca, N., & Šmuc, T. (2011). REVIGO summarizes and visualizes
1021 long lists of gene ontology terms. *Plos One, 6*, e21800.
1022 doi:10.1371/journal.pone.0021800
1023 Taberlet, P., & Bouvet, J. (1994). Mitochondrial DNA polymorphism, phylogeography,
1024 and conservation genetics of the brown bear Ursus arctos in Europe. *Proceeding*
1025 *of the Royal Society of London serie B, 255*, 195-200. doi:10.1098/rspb.1994.0028
1026 Tegelstrom, H. (1987). Transfer of mitochondrial DNA from the northern red-backed
1027 vole (*Clethrionomys rutilus*) to the bank vole (*C. glareolus*). *Journal of Molecular*
1028 *Evolution, 24*, 218-227. doi:10.1007/BF02111235
1029 Tegelstrom, H., & Jaarola, M. (1998). Geographic localization of a contact zone between
1030 bank voles *Clethrionomys glareolus* with distinctly different mitochondrial DNA.
1031 *Acta Theriologica, 43*, 175-183. doi:10.4098/AT.arch.98-13
1032 Vatsiou, A. I., Bazin, E., & Gaggiotti, O. E. (2016). Changes in selective pressures
1033 associated with human population expansion may explain metabolic and immune
1034 related pathways enriched for signatures of positive selection. *BMC Genomics, 17*,
1035 11. doi:10.1186/s12864-016-2783-2
1036 Vitalis, R., Gautier, M., Dawson, K. J., & Beaumont, M. A. (2014). Detecting and measuring
1037 selection from gene frequency data. *Genetics, 196*, 799-817.
1038 doi:10.1534/genetics.113.152991

1039 Wenzel, M. A., Douglas, A., James, M. C., Redpath, S. M., & Piertney, S. B. (2016). The role
1040 of parasite-driven selection in shaping landscape genomic structure in red grouse
1041 (*Lagopus lagopus scotica*). *Molecular Ecology, 25*, 324-341.
1042 doi:10.1111/mec.13473
1043 White, B. J., Lawniczak, M. K. N., Cheng, C. D., Coulibaly, M. B., Wilson, M. D., Sagnon, N., . . .
1044 Besansky, N. J. (2011). Adaptive divergence between incipient species of
1045 *Anopheles gambiae* increases resistance to Plasmodium. *Proceedings of the*
1046 *National Academy of Sciences of the United States of America, 108*, 244-249.
1047 doi:10.1073/pnas.1013648108
1048 Yanagihara, R., & Silverman, D. J. (1990). Experimental infection of human vascular
1049 endothelial cells by pathogenic and non pathogenic hantaviruses *Archives of*
1050 *Virology, 111*, 281-286. doi:10.1007/bf01311063
1051 Yang, X. N., Yang, H. L., Zhou, G. Q., & Zhao, G. P. (2008). Infectious disease in the genomic
1052 era. In *Annual Review of Genomics and Human Genetics* (Vol. 9, pp. 21-48). Palo
1053 Alto: Annual Reviews.
1054 Zeimes, C. B., Olsson, G. E., Ahlm, C., & Vanwambeke, S. O. (2012). Modelling zoonotic
1055 diseases in humans: comparison of methods for hantavirus in Sweden.
1056 *International Journal of Health Geographics, 11*. doi:10.1186/1476-072x-11-39
1057 Zeimes, C. B., Quoilin, S., Henttonen, H., Lyytikaïnen, O., Vapalahti, O., Reynes, J. M., . . .
1058 Vanwambeke, S. O. (2015). Landscape and regional environmental analysis of the
1059 spatial distribution of hantavirus human cases in Europe. *Frontiers in Public*
1060 *Health, 3*, 1-10. doi:10.3389/fpubh.2015.00054
1061

1062 **Data accessibility**

DNA sequences of candidate genes are accessible in Genbank (see accession numbers in Table 3).

Illumina RAD-tag sequences will be accessible in dryad digital depository.

Our final SNP data set is available as a supplementary file.

Author contribution

A.R., M.Gal. and N.C. designed the research. G. O. performed field sampling. A.R., M.Gal. and K.G. performed the laboratory work. N.C., A.R., B.G., R.V. and M.Gau. helped with bioinformatics and statistical analyses, C.Z. and S.VW provided the environmental data. N.C. wrote the first draft of the manuscript, and all authors contributed substantially to revisions.

Fig. 1 Maps showing the localities of bank vole sampling in Sweden. The red lines delimit the counties with 90% of human hantavirus cases reported. Geographic variations in ecoregions are represented with yellow, orange and green colors. The contact zone between the two mitochondrial lineages of *M. glareolus* is indicated with a black line.

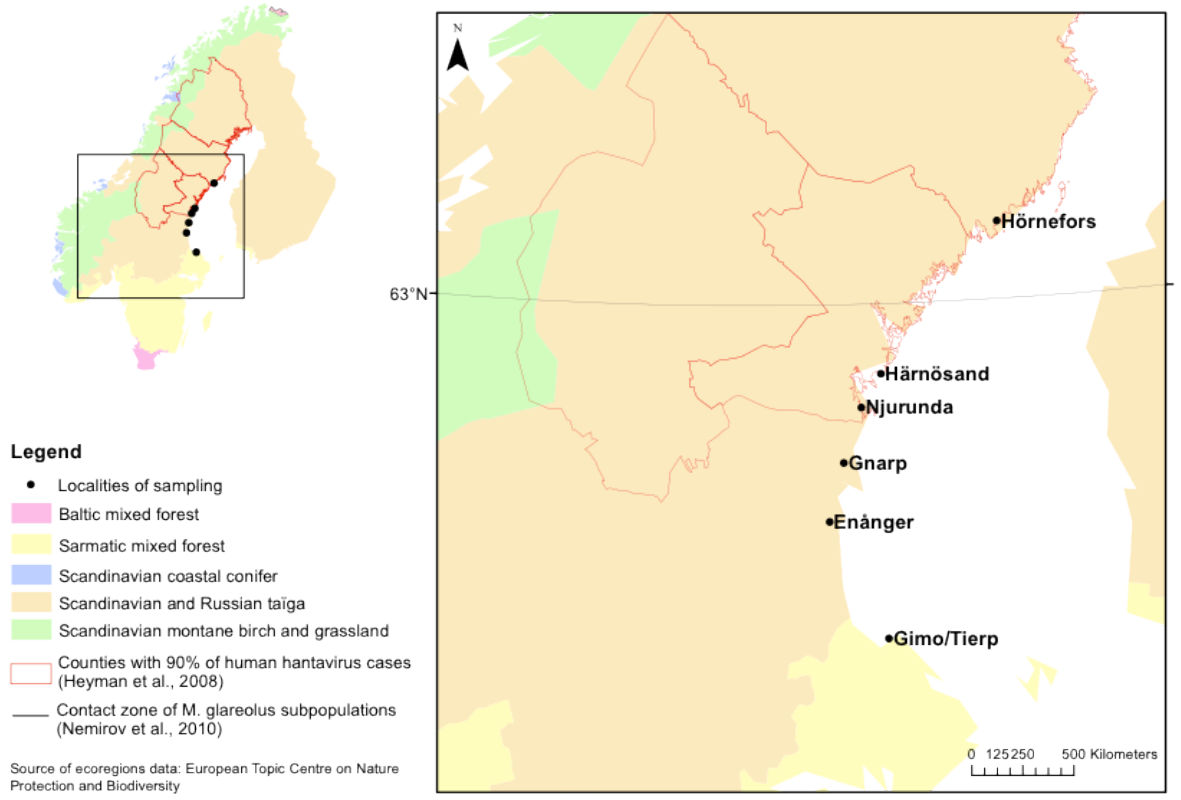

Fig. 2 Principal Component Analysis (PCA) plot of the environmental data and of the six populations analysed. Details about envionmental variables are provided in Table 2.

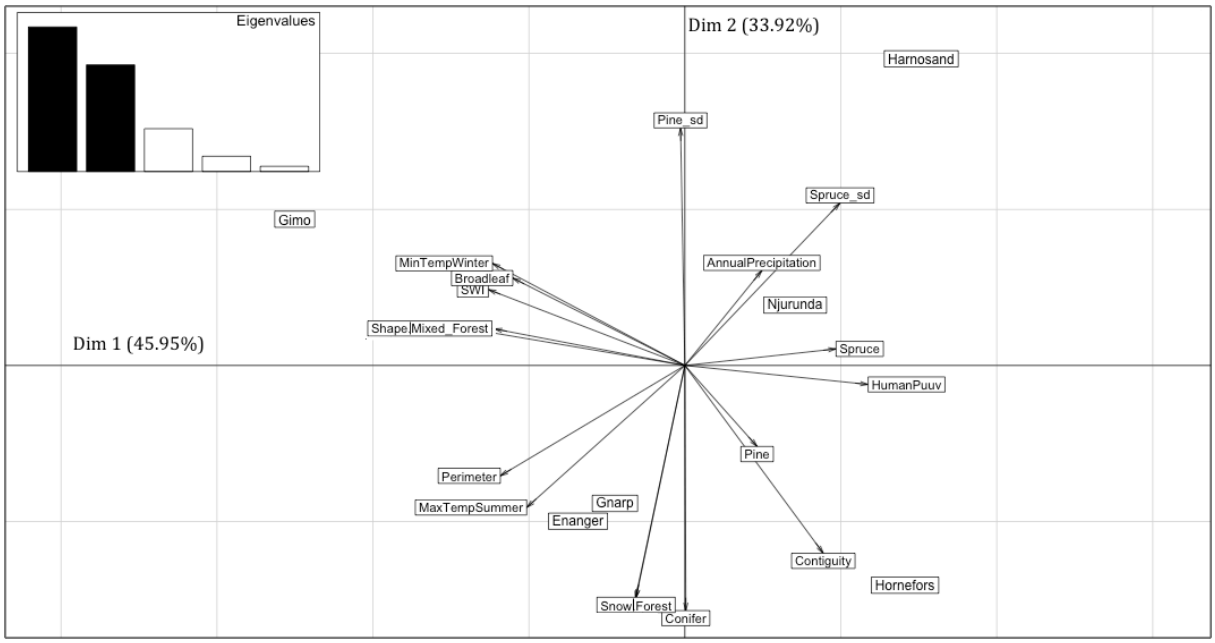

Fig. 3 Graphical representations of the *M. glareolus* population genetic structure based on the 95,988 SNPS. a) Principal Component Analysis (PCA) based on the variance covariance matrix of the six bank vole populations studied, estimated using BAYPASS and based on the 95,988 SNPs included in the statistical analyses. b) Representation of the scaled covariance matrice as estimated from BAYPASS under the core model with $\rho = 1$. c) Isolation by distance pattern.

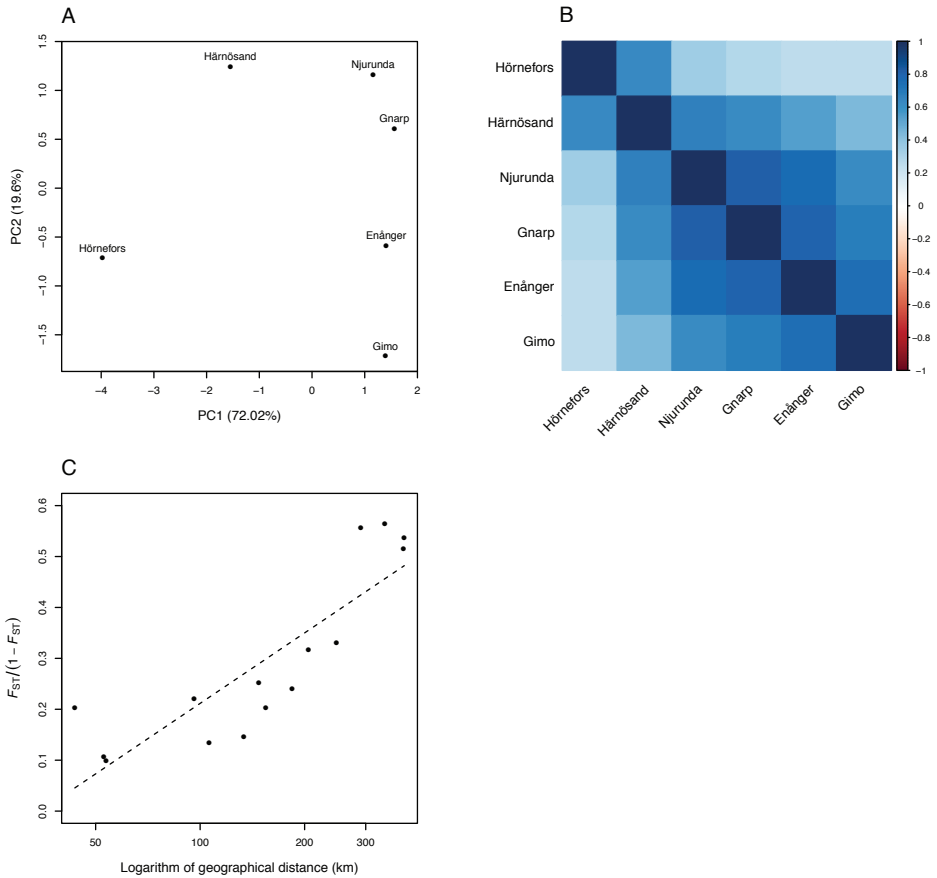

Fig. 4 Outlier detection based on 95,988 SNPs in the six bank vole populations using SELESTIM. a) F_{ST} estimates are represented as a function of the Kullback-Leibler Divergence (KLD) measure for all SNPs. Vertical lines correspond to the 99.90, 99.95 and 99.99 % quantiles calculated from the KLD calibration procedure. b) Correlations between the locus- and population-specific coefficient of selection and the coordinates of the first principal components of the environmental variables. The colored lines stand for outlier SNPs, and the thin grey lines stand for all markers. The coefficient of selection was transformed as: 2 * \sigma_{ij} * (\kappa_{ij} – 0.5).

a)

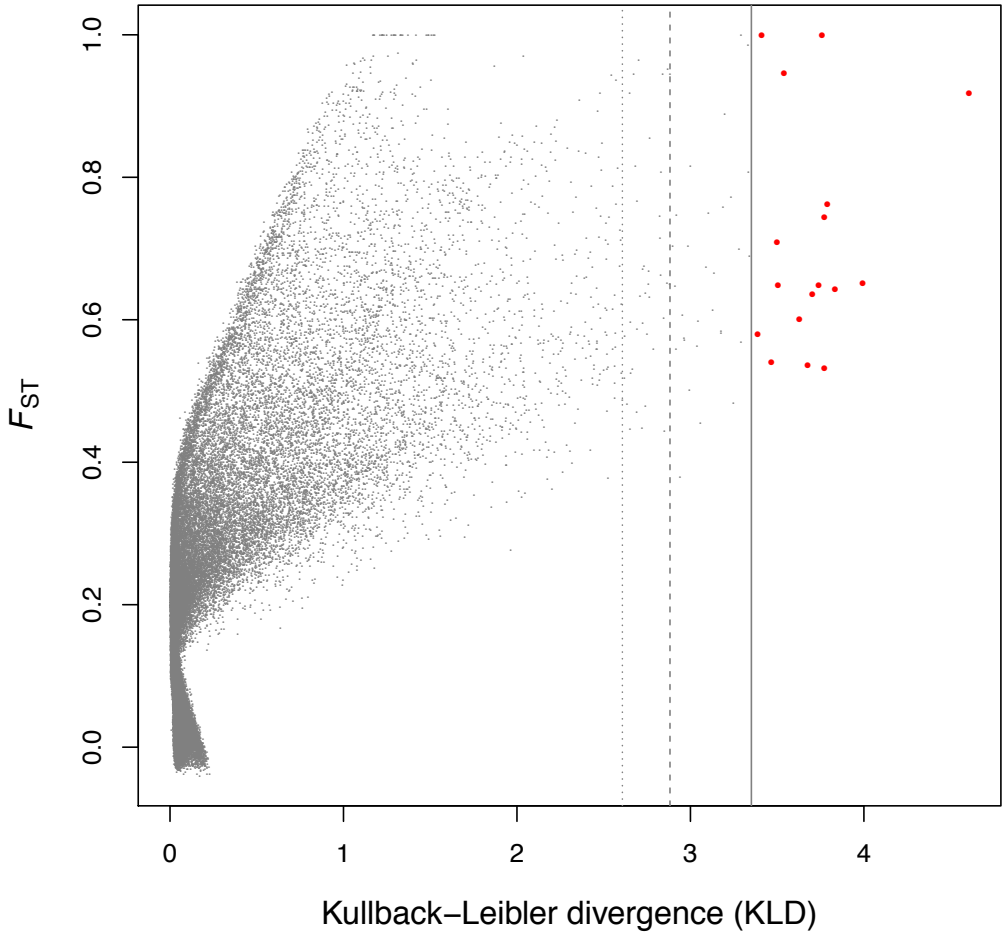

b)

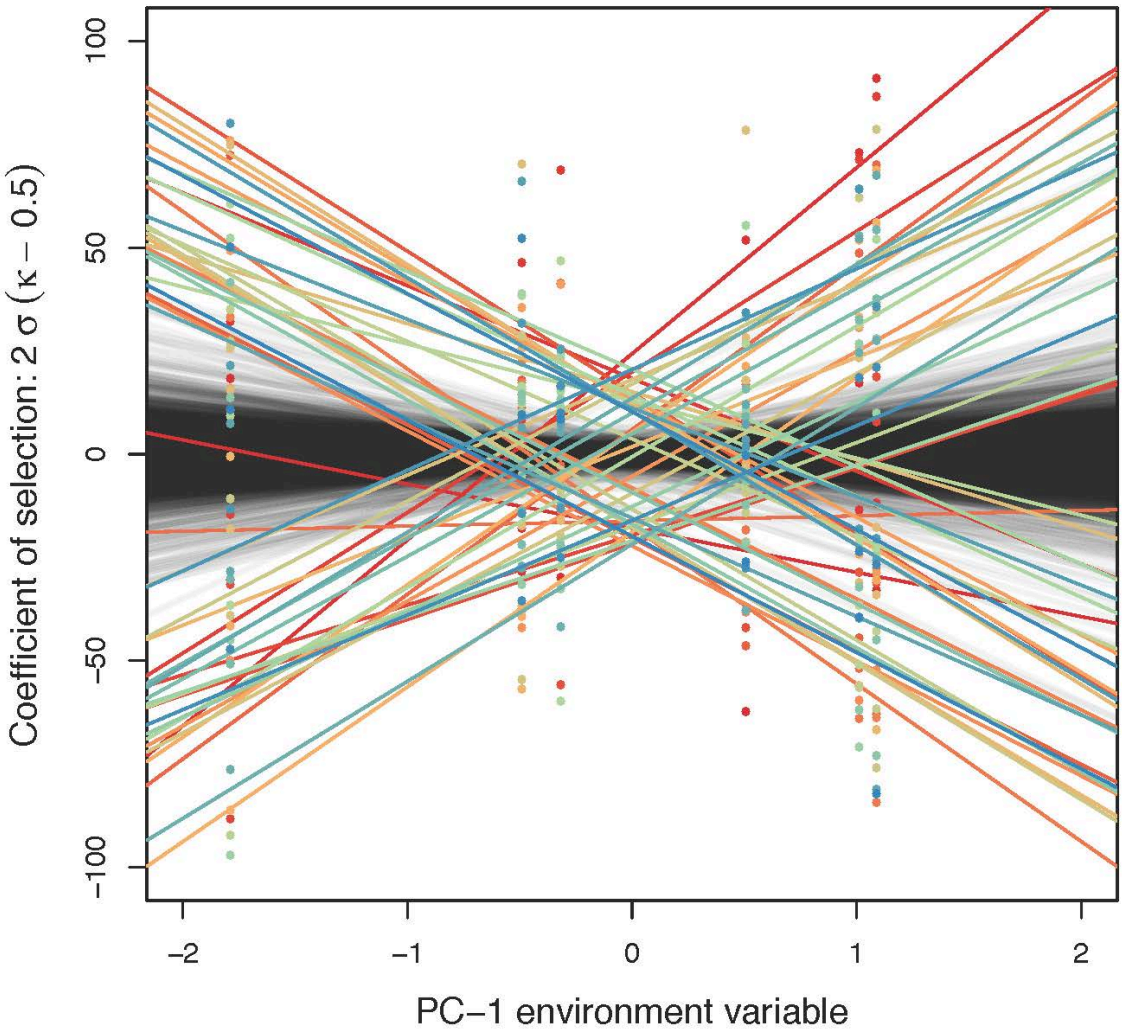

31
32

Fig. 5 Outlier detection based on 95,988 SNPs in the six bank vole populations using BAYPASS. a) Correlation between Kullbac-Leibler Divergence (KLD) measure for all SNPs and the statistics X^TX estimated using BAYPASS. Horizontal lines correspond to the 99.90, 99.95 and 99.99 % quantiles calculated from the KLD calibration procedure. Vertical lines correspond to these three quantiles calculated using simulations from a predictive distribution based on the observed dataset. b) Correlation between the statistics *eBP* (with the environmental synthethic variable being PCA axis 1) and X^TX estimated using BAYPASS. Horizontal and vertical lines correspond to the 99.90, 99.95 and 99.99 % quantiles calculated from the simulations described above. c) Correlation between the statistics *eBP* (with the environmental synthethic variable being PCA axis 2) and X^TX estimated using BAYPASS. Horizontal and vertical lines correspond to the 99.90, 99.95 and 99.99 % quantiles calculated from the simulations described above.

a)

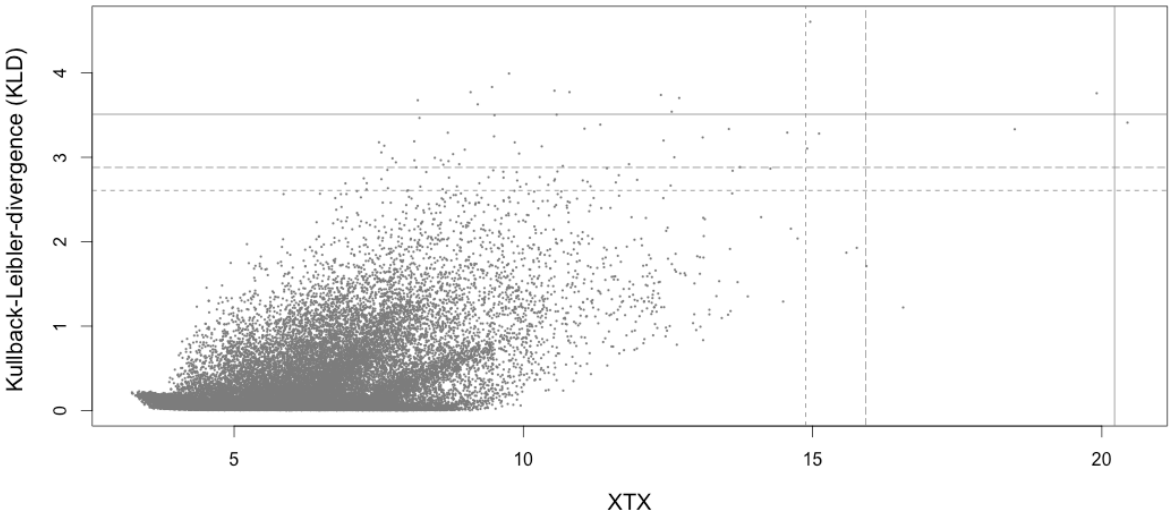

b)

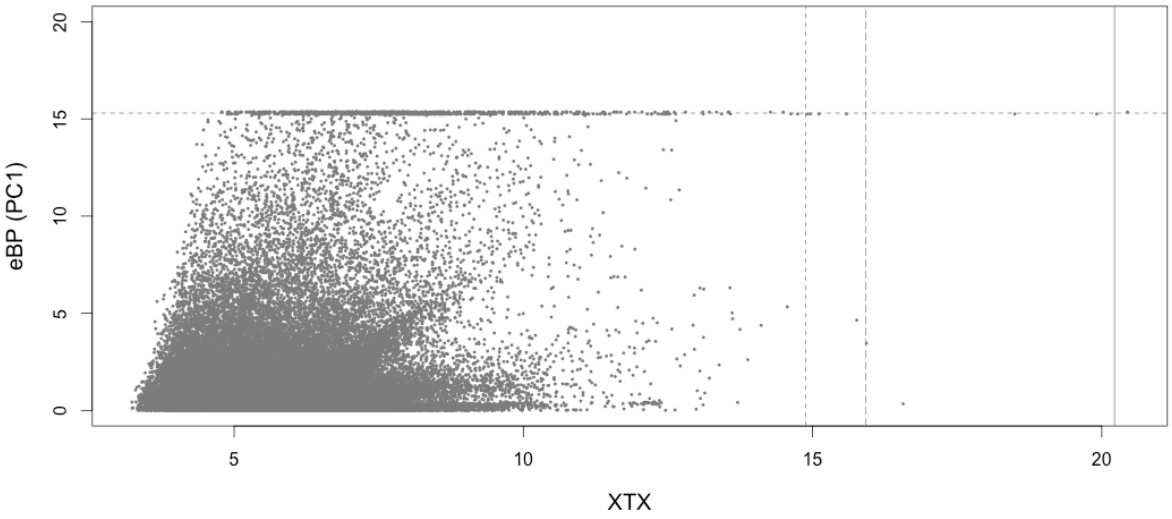

c)

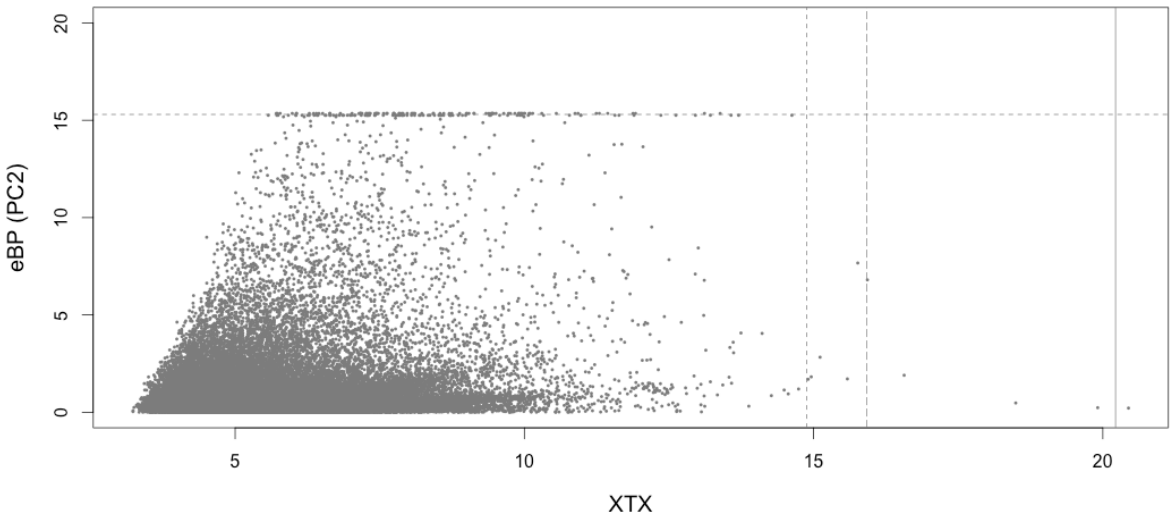

51
52

Fig. 6. Gene network obtained with STRING including the 52 outliers with annotation based on *M. musculus* genome. Small nodes indicate proteins of unknown 3D structure. Edges represent protein-protein associations based on known interactions (blue: from curated databases; pink: experimentally tested, black= co-expression) or predicted ones (green= gene neighborhood).

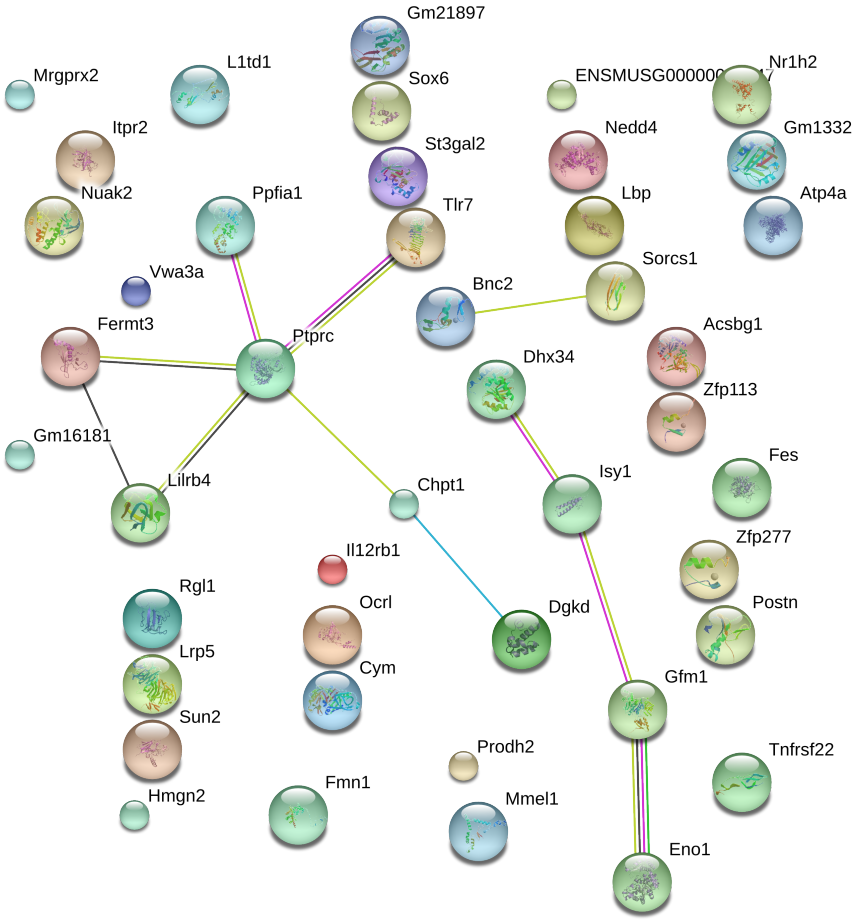

Fig. 7 TreeMap view of REVIGO Biological Process analyses. Each rectangle represents a single cluster, that are grouped into 'superclusters' of related terms, represented with different colors. The size of the rectangles reflects the frequency of the GO term in the set of outliers included in this analysis.

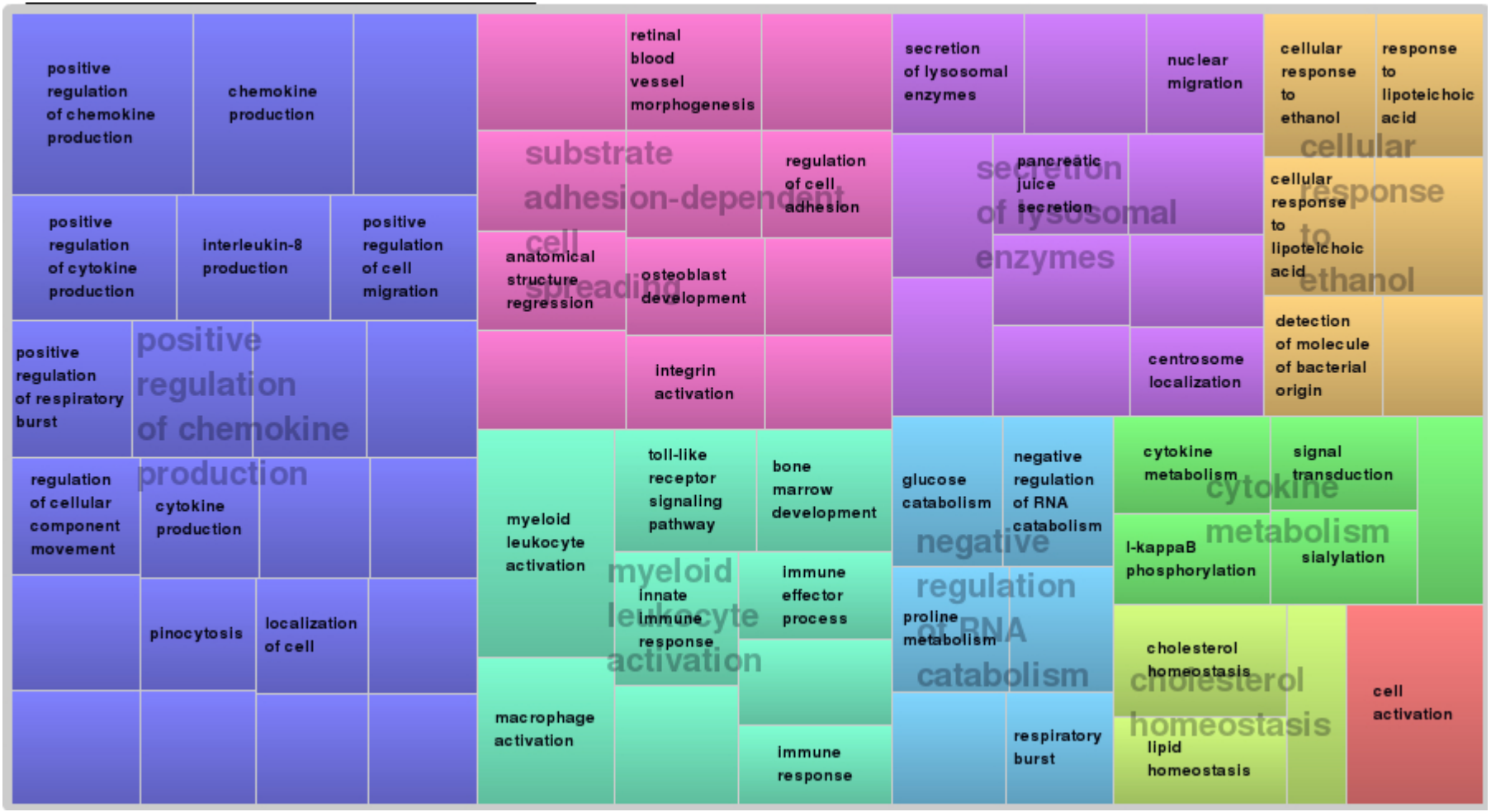

Table 1. Sampling information, including localities of sampling and their administrative county, geographic coordinates (centre point from where the voles are trapped, voles are all caught within 1 kilometer from that point), the number of voles trapped *N*, the date of sampling, and the minimum, maximum and total number of human cases reported per county between 2001 and 2011 (SMI data).

Localities	County	Latitude	Longitude	*N*	Date of sampling	PUUV – Human cases Min / Max / Total / Pop. size
Hörnefors	Västerbotten	N 63° 33’ 50’’	E 19° 47’ 20’’	49	April 2012	13 / 808 / 2152 / 259,239
Härnösand	Västerbotten	N 62° 29’ 30’’	E 17° 49’ 00’’	57	April 2012	13 / 808 / 2152 / 259,239
Njurunda	Vasternorrland	N 62° 15’ 15’’	E 17° 29’ 45’’	20	April 2012	14 / 391 / 1289 / 242,347
				14	October 2012	
Gnarp	Gävleborg	61° 51’ 15’’	17° 12’ 10’’	47	October 2012	4 / 58 / 219 / 276,323
Enånger	Gävleborg	61° 25’ 25’’	16° 57’ 58’’	28	October 2012	4 / 58 / 219 / 276,323
Gimo	Uppsala	60° 33’ 36’’	17° 50’ 06’’	25	April 2012	1 / 15 / 95 / 200,032
				17	October 2012	

6 **Table 2**. Environmental parameters and their potential impacts (indicated by 'x') on the bank voles' abundance or virus survival outside
7 the host (see Zeimes et al., 2015 for references).
8

Variables	Bank voles	Virus	Resolution	Units	Sources
PUUV presence					
Total number of human cases between 2001 and 2011 (SWI dataset)		x	County		
Climatic variables					
Minimum temperature in winter (MinTempWinter)	x	x	0.0083° 1950-2000	°C	Worldclim
Maximum temperature in summer (MaxTempSummer)		x	0.0083° 1950-2000	°C	Worldclim
Snow cover (Snow)	x	x	0.005° 2000-2008	Area percentage	MODIS
Annul precipitation (Pp)	x	x	0.0083°	mm	Worldclim

			1950-2000		
Forest and soil indices					
Proportion of forest	x		100 m	Area percentage	Corine 2006 (EEA)
Proportion of broadleaved forest	x		100 m	Area percentage	Corine 2006 (EEA)
Proportion of coniferous forest	x		100 m	Area percentage	Corine 2006 (EEA)
Proportion of mixed forest	x		100 m	Area percentage	Corine 2006 (EEA)
Mean volume of spruce	x		25 m	m^3/ha	SLU Skogskarta
Standard deviation of the volume of spruce	x		25 m	m^3/ha	SLU Skogskarta
Mean volume of pine	x		25 m	m^3/ha	SLU Skogskarta
Standard deviation of the volume of pine	x		25 m	m^3/ha	SLU Skogskarta
Average contiguity index of forest patches	x		1:20000	Relative unit	Lantmäteriet
Average shape index of forest patches	x		1:20000	Relative unit	Lantmäteriet
Perimeter of the forest patches	x		1:20000	m	Lantmäteriet
Soil water index (SWI)	x	x	25 km 2007-2010	Relative unit	TU-WIEN

9

Table 3. Summary of sequenced candidate immune-related genes of bank voles (n=12). More details about these SNPs are provided in Table S3. * This insertion/deletion was only polymorph in Germany. ** one was not genotyped because of 100% LD with the other one, the non synonymous SNP was only polymorph in France. *** The other SNPs were either only detected in one individual from France or only detected in Germany. **** Only one SNP shown to be involved in PUUV / *M. glareolus* interaction (Guivier et al., 2014; Guivier et al., 2010) was genotyped.

Gene name	Description of gene function	Fragment length / Total length	SNP detected*	SNP genotyped	Genbank
Myxovirus resistance (Mx2)	Interferon-induced antiviral protein				
exon 13		226 / 246	1	0*	KX463515 - KX463526
exon 14		205 / 237	3	1**	KX463527 - KX463563
Toll-like receptor 4 (Tlr4)	Pattern-recognition receptor; primarily recognizes LPS				
exon 3		1888 / 2843	14	5***	KX463564 - KX463604
Toll-like receptor 7	Pattern-recognition				

(Tlr7) exon 3	receptor; primarily recognizes ss RNA virus genomes	2916 / 3153	1	1	KX463605 - KX463616
Tumor necrosis factor alpha (*Tnf*) promoter	Cytokine involved in pro-inflammatory immune response	560 / 644	7	1****	HM107872.1

Table 4. Diversity indices per sampling locality and SNP. Values in bold indicate significant *p*-values.

		Localities					
		Hörnesand	Härneförs	Njurunda	Gnarp	Enånger	Gimo
SNP	Indices						
Mx2_14_162	He n.b.	0.4639	0.1759	0.000	0.000	0.000	0.000
	Hobs.	0.4694	0.1579	0.000	0.000	0.000	0.000
	Fis W.C.	-0.012	0.103	-	-	-	-
TLR4_667	He n.b.	0.000	0.000	0.0294	0.1311	0.1726	0.5065
	Hobs.	0.000	0.000	0.0294	0.1389	0.1875	0.2703
	Fis W.C.	-	-	0.000	-0.061	-0.088	**0.470**
TLR4_776	He n.b.	0.0600	0.0517	0.2950	0.4261	0.4583	0.2755
	Hobs.	0.0612	0.0526	0.2941	0.4286	0.5000	0.1622
	Fis W.C.	-0.021	-0.018	0.003	-0.006	-0.093	**0.415**
TLR4_1146	He n.b.	0.0791	0.0517	0.2950	0.4409	0.4583	0.2755
	Hobs.	0.0816	0.0526	0.2941	0.4167	0.5000	0.1622
	Fis W.C.	-0.032	-0.018	0.003	0.056	-0.093	**0.415**
TLR4_1662	He n.b.	0.0600	0.0517	0.3021	0.4343	0.4583	0.2936
	Hobs.	0.0612	0.0526	0.3030	0.4054	0.5000	0.1892
	Fis W.C.	-0.021	-0.018	-0.003	0.067	-0.093	**0.359**
TLR4_1687	He n.b.	0.0412	0.0517	0.2950	0.4409	0.4583	0.2755
	Hobs.	0.0417	0.0526	0.2941	0.4167	0.5000	0.1622
	Fis W.C.	-0.011	-0.018	0.003	0.056	-0.093	**0.415**
TLR7_2593	He n.b.	0.0000	0.3552	0.1383	0.4261	0.5079	0.0000
	Hobs.	0.0000	0.1404	0.1471	0.3143	0.3750	0.0000
	Fis W.C.	-	**0.607**	-0.065	0.265	0.265	-
TNFp_296	He n.b.	0.4033	0.4988	0.3652	0.2950	0.2285	0.4832
	Hobs.	0.0204	0.0175	0.1765	0.2941	0.1935	0.2432
	Fis W.C.	**0.950**	**0.965**	**0.521**	0.003	0.155	**0.500**

Table 5. Outlier SNPs identified using at least one of the three methods implemented to detect signatures of selection : SelEstim, BayPass and BayPass with environmental variables (respectively when associations were found with PC1 or PC2). Only SNPS that belonged to contigs that aligned to the mouse genome and corresponded to genes coding for proteins are included here. Gene name and description were obtained in Pathway are indicated following KEGG or Reactom results. Genes related to immunity are indicated by *. Those related to metabolism processes are indicated by #.

Gene ID (Ensembl)	SNP (MRK_RAD)	Consensus Sequence	Gene abbreviation and synonyms	Gene name and description	Method of outlier detection	Pathway
ENSMUSG000000094472	61 62	C100162	Gm21897	Uncharacterized protein	KLD X^TX eBP-1	-
#ENSMUSG00000003038	84025	C7205	Hmgn2, HMG-17, Hmg17	High mobility group nucleosomal binding	KLD	Metabolic pathways Glycerophospholipid

				inner side of the nucleosomal DNA thus altering the interaction between the DNA and the histone octamer		Choline metabolism in cancer Ether lipid metabolism
ENSMUSG00000006019	55395	C261693	Dhx34, 1200013B07Rik, 1810012L18Rik, Ddx34, mKIAA0134	DEAH (Asp-Glu-Ala-His) box polypeptide 34; Probable ATP-binding RNA helicase	KLD	-
*ENSMUSG00000010751	34586	C194382	Tnfrsf22, 2810028K06Rik, C130035G06Rik, SOBa, Tnfrh2, Tnfrsf1al2, mDcTrailr2	Tumor necrosis factor receptor superfamily, member 22; Receptor for the cytotoxic ligand TNFSF10/TRAIL. Protects cells against TRAIL	KLD	-

				mediated apoptosis		
*ENSMUSG00000026395	13196	C134235	Ptprc, B220, CD45R, Cd45, L-CA, Ly-5, Lyt-4, T200, loc	Protein tyrosine phosphatase, receptor type, C; Protein tyrosine-protein phosphatase required for T-cell activation through the antigen receptor.	KLD	Cell adhesion molecules (CAMs) Fc gamma R-mediated phagocytosis T cell receptor signaling pathway
ENSMUSG00000026482	35102	C195922	Rgl1, Rgl, mKIAA0959	Ral guanine nucleotide dissociation stimulator,-like 1; Probable guanine nucleotide exchange factor	KLD	Metabolism Ras signaling pathway
#ENSMUSG00000032281	23560	C161736	Acsbg1, BG1, Bgm, E230019G03Rik, Lpd, R75185,	Acyl-CoA synthetase bubblegum family member 1; Mediates activation of long-chain fatty acids for	KLD	Metabolic pathways Fatty acid metabolism Adipocytokine

			mKIAA0631	both synthesis of cellular lipids, and degradation via beta-oxidation		signaling pathway Fatty acid degradation
ENSMUSG00000051910	59381	C276731	Sox6, AI987981, SOX-LZ	SRY-box containing gene 6; Transcriptional activator. Plays a key role in several developmental processes,	KLD	-
ENSMUSG00000053158	12626	C132789	Fes, AI586313, BB137047, FPS, c-fes	Feline sarcoma oncogene; Tyrosine-protein kinase that acts downstream of cell surface receptors and plays a role in the regulation of the actin cytoskeleton, microtubule assembly, cell attachment and cell spreading	KLD	Axon guidance

ENSMUSG00000024913	62875	C290668	Lrp5, BMND1, HBM, LR3, LRP7, OPPG, mKIAA4142	Low density lipoprotein receptor-related protein 5; Component of the Wnt-Fzd-LRP5-LRP6 complex that triggers beta-catenin signaling through inducing aggregation of receptor-ligand complexes into ribosome-sized signalsomes.	KLD eBP-1	Wnt signaling pathway
ENSMUSG00000043531	32706 86077	C188407 C76715	Sorcs1, Sorcs, mSorCS	VPS10 domain receptor protein SORCS 1	KLD eBP-1	-
ENSMUSG00000044583		Candidate gene	Tlr7	Toll-like receptor 7; Key component of innate and adaptive immunity	KLD eBP-1	Toll receptor signaling pathway

*ENSMUSG00000000791	89604	C84915	Il12rb1, CD212, IL-12R[b]	Interleukin 12 receptor, beta 1; Functions as an interleukin receptor which binds interleukin-12 with low affinity and is involved in IL12 transduction	eBP-1	Cytokine-cytokine receptor interaction Jak-STAT signaling pathway Interleukin signaling pathway
#ENSMUSG00000001173	38137 48974 51765 69107 83890	C204541 C239849 C248728 C37197 C71726	Ocrl, 9530014D17Rik, BB143339, OCRL1	Oculocerebrorenal syndrome of Lowe; Converts phosphatidylinositol 4,5-bisphosphate to phosphatidylinositol 4-phosphate	eBP-1	Metabolic pathways Inositol phosphate metabolism Phosphatidylinositol signaling system
#ENSMUSG00000005553	66006	C30857	Atp4a	ATPase, H+/K+ exchanging, gastric, alpha polypeptide; Catalyzes the hydrolysis of	eBP-1	Oxidative phosphorylation Gastric acid

				ATP coupled with the exchange of H(+) and K(+) ions across the plasma membrane		secretion Collecting duct acid secretion
#ENSMUSG00000009772	53579	C255238	Nuak2, 1200013B22Rik, Omphk2, Snark, mKIAA0537	NUAK family, SNF1-like kinase, 2; Stress-activated kinase involved in tolerance to glucose starvation.	eBP-1	
*ENSMUSG00000016024	94448	C96304	Lbp, Bpifd2, Ly88	Lipopolysaccharide binding protein; Binds to the lipid A moiety of bacterial lipopolysaccharides (LPS) and acts as an affinity enhancer for CD14.	eBP-1	NF-kappa B signaling pathway Toll-like receptor signaling pathway Salmonella infection Tuberculosis
*ENSMUSG00000024965	71214	C41693	Fermt3, C79673,	Fermitin family homolog 3	eBP-1	Platelet activation

			Kindlin3	(Drosophila); Plays a central role in cell adhesion in hematopoietic cells. Acts by activating the integrin beta-1-3 required for integrin-mediated platelet adhesion and leukocyte adhesion to endothelial cells.		
ENSMUSG00000027750	47669	C235550	Postn, A630052E07Rik, AI747096, OSF-2, Osf2, PLF, PN, peri	Periostin, osteoblast specific factor; Induces cell attachment and spreading and plays a role in cell adhesion.	eBP-1	-
ENSMUSG00000027774	10489-97	C12723	Gfm1	G elongation factor, mitochondrial 1.	eBP-1	

ENSMUSG00000028487	5793	C114918	Bnc2	Basonuclin 2; Probable transcription factor specific for skin keratinocytes.	eBP-1	
ENSMUSG00000030056	23902	C162542	Isy1, 5830446M03Rik, AI181014, AU020769	ISY1 splicing factor homolog (*S. cerevisiae*); May play a role in pre-mRNA splicing	eBP-1	Spliceosome
#ENSMUSG00000031749	26707	C170555	St3gal2, AI429591, AW822065, ST3GalII, Siat5	ST3 beta-galactoside alpha-2,3-sialyltransferase 2.	eBP-1	Metabolic pathways Glycosphingolipid biosynthesis Glycosaminoglycan biosynthesis
*ENSMUSG00000032216	48950	C23976	Nedd4, AA959633, AL023035, AU019897,	Neural precursor cell expressed, developmentally down-regulated 4; E3 ubiquitin-protein ligase	eBP-1	Immune System Ubiquitin mediated proteolysis Epstein-Barr virus

			E430025J12Rik, Nedd4-1, Nedd4a, mKIAA0093	which accepts ubiquitin from an E2 ubiquitin-conjugating enzyme in the form of a thioester and then directly transfers the ubiquitin to targeted substrates.		infection
#ENSMUSG00000036892	91136	C88644	Prodh2, 2510028N04Rik, 2510038B11Rik, MmPOX, MmPOX1, POX1	Proline dehydrogenase (oxidase) 2; Converts proline to delta-1-pyrroline-5-carboxylate	eBP-1	Metabolic pathways Arginine and proline metabolism
ENSMUSG00000037519	86924	C78794	Ppfia1, C030014K08Rik, C87158, LIP.1, LIP1	Protein tyrosine phosphatase, receptor type, f polypeptide (PTPRF), interacting protein (liprin),	eBP-1	Neuronal System Transmission across Chemical Synapses

				alpha 1		
ENSMUSG00000042524	37922	C203929	Sun2, B230369L08Rik, C030011B15, Unc84b	Sad1 and UNC84 domain containing 2; Component of SUN-protein-containing multivariate complexes also called LINC complexes which link the nucleoskeleton and cytoskeleton by providing versatile outer nuclear membrane attachment sites for cytoskeletal filaments	eBP-1	Meiotic synapsis Cell Cycle Meiosis
ENSMUSG00000044042	42927-8	C21976	Fmn1	Formin 1; Plays a role in the formation of adherens junction and the polymerization of linear	eBP-1	-

				actin cables.		
ENSMUSG00000055917	2024 20453 78750	C105390 C153598 C59434	Zfp277, 2410017E24Rik, NIRF4	Zinc finger protein 277	EpBPis1	-
ENSMUSG00000057047	21103	C15518	1700010B08Rik	RIKEN cDNA 1700010B08 gene	eBP-1	-
ENSMUSG00000058183	14341	C13737	Mmel1, Mell1, NEP2, NEPII, Nl1, SEP	Membrane metallo-endopeptidase-like 1; Metalloprotease involved in sperm function, possibly by modulating the processes of fertilization and early embryonic developmen	eBP-1	-
#ENSMUSG00000060002	39654 43056	C209068 C220188	Chpt1	Choline phosphotransferase 1;	eBP-1	Metabolic pathways Glycerophospholipid

				Catalyzes phosphatidylcholine biosynthesis from CDP-choline.		metabolism Ether lipid metabolism
ENSMUSG00000060601	83851	C71650	Nr1h2, AI194859, LXR, LXRB, LXRbeta, NER1, OR-1, RIP15, UR, Unr, Unr2	Nuclear receptor subfamily 1, group H, member 2; Regulates cholesterol uptake through MYLIP-dependent ubiquitination of LDLR, VLDLR and LRP8; DLDLR and LRP8	eBP-1	Nuclear Receptor transcription pathway Generic Transcription Pathway Gene Expression
#ENSMUSG00000063524	84862	C73976	Eno1, 0610008I15, AL022784, Eno-1, MBP-1	Enolase 1, alpha non-neuron; Multifunctional enzyme that, as well as its role in glycolysis, plays a part in various processes	eBP-1	HIF-1 signaling pathway Metabolic pathways Carbon metabolism Biosynthesis of

				such as growth control, hypoxia tolerance and allergic responses		amino acids Glycolysis / Gluconeogenesis
*ENSMUSG00000070738	71571	C42550	Dgkd, AI841987, D330025K09, DGKdelta, dgkd-2	Diacylglycerol kinase, delta	eBP-1	Metabolic pathways Glycerolipid metabolism Glycerophospholipid metabolism Phosphatidylinositol signaling system Platelet activation, signaling and aggregation
ENSMUSG00000074109	35853	C198117	Mrgprx2, G370024M05Rik, MrgB10,	MAS-related GPR, member X2; Probably involved in the function of nociceptive	eBP-1	-

			Mrgprb10	neurons.		
ENSMUSG00000074628	43497	C22169	Tldc2, Gm1332	TBC/LysM-Associated Domain Containing 2	eBP-1	-
ENSMUSG00000081650	16184	C141730	Gm16181	Predicted gene 16181	eBP-1	
ENSMUSG00000046213	70760	C40587	Cym, Gm131	Chymosin	eBP-1 eBP-2	-
#ENSMUSG00000030287	56067	C264313	Itpr2, AI649341, InsP3R-2, InsP3R-5, Ip3r2, Itpr5, insP3R2	Inositol 1,4,5-triphosphate receptor 2; Receptor for inositol 1,4,5-trisphosphate, a second messenger that mediates the release of intracellular calcium	eBP-2	Thyroid hormone synthesis Gastric acid secretion Pancreatic secretion Phosphatidylinositol signaling system
*ENSMUSG00000030889	13626	C135480	Vwa3a, E030013G06Rik	von Willebrand factor A domain containing 3A	eBP-2	Pathways in cancer MAPK signaling

						pathway TNF signaling pathway Ras signaling pathway Toll-like receptor signaling pathway FoxO signaling pathway RIG-I-like receptor signaling pathway
#ENSMUSG00000037007	91750	C90068	Zfp113, 4732456B05Rik, mKIAA4229	zinc finger protein 113	eBP-2	Metabolism Metabolic disorders of biological oxidation enzymes

						Fatty acids Biological oxidations
*ENSMUSG00000062593	62536	C289384	Lilrb4, CD85K, Gp49b, HM18, ILT3, LIR-5, gp49	Leukocyte immunoglobulin-like receptor, subfamily B, member 4; Receptor for class I MHC antigens. Involved in the down-regulation of the immune response and the development of tolerance.	eBP-2	Immune system
ENSMUSG00000087166	44693	C225538	L1td1, AA546746, AB211064, D76865, ECAT11	LINE-1 type transposase domain containing 1	eBP-2	-